Available online at www.sciencedirect.com
SCIENCE DIRECT®
ELSEVIER
Physics of the Earth and Planetary Interiors 140 (2003) 219–242
PHYSICS OF THE EARTH AND PLANETARY INTERIORS
www.elsevier.com/locate/pepi

D″ shear velocity heterogeneity, anisotropy and discontinuity structure beneath the Caribbean and Central America

Edward J. Garnero[a,*], Thorne Lay[b,1]

[a] Department of Geological Sciences, Arizona State University, Tempe, AZ 85284, USA
[b] University of California, Santa Cruz, Santa Cruz, CA, USA

Accepted 11 July 2003

Abstract

The D″ region in the lowermost mantle beneath the Caribbean and Central America is investigated using shear waves from South American earthquakes recorded by seismic stations in North America. We present a large-scale, composite study of volumetric shear velocity heterogeneity, anisotropy, and the possible presence of a D″ discontinuity in the region. Our data set includes: 328 $S(S_{\mathrm{diff}})$-*SKS* differential travel times, 300 *ScS*-*S* differential travel times, 125 $S(S_{\mathrm{diff}})$ and 120 *ScS* shear wave splitting measurements, and 297 seismograms inspected for *Scd*, the seismic phase refracted from a high-velocity D″ layer. Broadband digital data are augmented by high-quality digitized analog WWSSN data, providing extensive path coverage in our study area. In all, data from 61 events are utilized. In some cases, a given seismogram can be used for velocity heterogeneity, anisotropy, and discontinuity analyses. Significant mid-mantle structure, possibly associated with the ancient subducted Farallon slab, affects shear wave travel times and must be corrected for to prevent erroneous mapping of D″ shear velocity. All differential times are corrected for contributions from aspherical mantle structure above D″ using a high-resolution tomography model. Travel time analyses demonstrate the presence of pervasive high velocities in D″, with the highest velocities localized to a region beneath Central America, approximately 500–700 km in lateral dimension. Short wavelength variability overprints this general high-velocity background. Corrections are also made for lithospheric anisotropy beneath the receivers. Shear wave splitting analyses of the corrected waveforms reveal D″ anisotropy throughout the study area, with a general correlation with heterogeneity strength. Evidence for *Scd* arrivals is pervasive across the study area, consistent with earlier work, but there are a few localized regions (100–200 km) lacking clear *Scd* arrivals, which indicates heterogeneity in the thickness or velocity gradients of the high-velocity layer. While small-scale geographic patterns of heterogeneity, anisotropy, and discontinuity are present, the details appear complex, and require higher resolution array analyses to fully characterize the structure. Explanations for the high-shear wave speeds, anisotropy, and reflector associated with D″ beneath the Caribbean and Central America must be applicable over a lateral scale of roughly 1500 km^2, the dimension over which we observe coherent wavefield behavior in the region. A slab graveyard appears viable in this regard.

Keywords: Shear velocity; Anisotropy; Core–mantle boundary; D″; Heterogeneity

1. Introduction

The core–mantle boundary (CMB) is the site of the largest density contrast within the planet, separating profoundly different environments, with vast

* Corresponding author. Tel.: +1-480-965-7653; fax: +1-480-965-8102.
E-mail addresses: garnero@asu.edu (E.J. Garnero), thorne@emerald.ucsc.edu (T. Lay).
[1] Tel.: +1-831-459-3164.

0031-9201/$ – see front matter © 2003 Elsevier B.V. All rights reserved.
doi:10.1016/j.pepi.2003.07.014

differences in flow velocities and physical properties, including a change from solid silicate rock to liquid iron alloy. As in the case of Earth's second largest density contrast, at the surface, a diverse array of chemical and dynamical complexities is likely to be found at the CMB. Abundant evidence has emerged for volumetric seismic wave velocity heterogeneity, shear velocity anisotropy, seismic wave scattering, and intermittent seismic velocity discontinuities within the D″ region at the base of the mantle (e.g., see reviews by Lay et al., 1998a,b; Wysession et al., 1998; Kendall, 2000; Garnero, 2000). However, the relationships between and fundamental nature of these complexities are still unresolved. Hence, we are motivated to better characterize the region using seismic methods, presently the most direct probe of the deep planet. Doing so is a first step in any effort to better understand the chemical and dynamical evolution of the deep mantle.

Herein we address D″ structure beneath the Caribbean, which has been characterized as having high-seismic shear wave velocities by several recent whole mantle global tomographic inversions (e.g., Masters et al., 2000; Ritsema and Van Heijst, 2000; Megnin and Romanowicz, 2000; Gu et al., 2001; Grand, 2002), by tomographic imaging of the deepest mantle layer (e.g., Kuo et al., 2000; Castle et al., 2000), and also by forward modeling analyses (e.g., Lay, 1983; Bokelmann and Silver, 1993; Valenzuela and Wysession, 1998; Tkalcic and Romanowicz, 2001; Wysession et al., 2001) using a variety of data sets and methods. This region is commonly characterized as having some of the highest D″ shear velocities on Earth, and is of particular interest because it underlies a region of plate convergence over the past 150 m.y. (e.g., see Grand et al., 1997; Lithgow-Bertelloni and Richards, 1998, and Fig. 1). The *P* velocity structure is less well resolved, but appears to be moderately high velocity as well (e.g., Van der Hilst et al., 1997; Karason and Van der Hilst, 2001). This is commonly attributed to lower mantle penetration of subducted slabs, giving rise to the idea of a slab graveyard beneath downwellings in a whole mantle convection system. Many other scenarios have also been put forth in the literature (e.g., see Albarede and Van Der Hilst, 1999; Tackley, 2000).

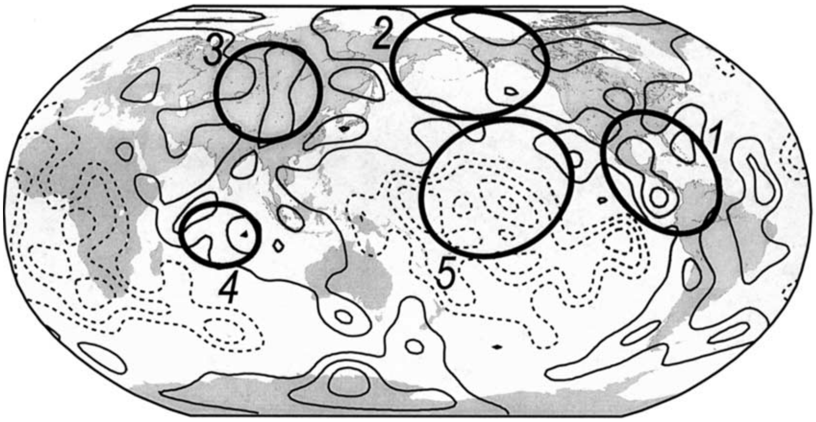

Fig. 1. Regions of past D″ studies documenting shear wave splitting caused by lowermost mantle anisotropy (thick lines). Lowermost mantle shear wave perturbations from Ritsema and Van Heijst (2000) are also displayed: the solid and dashed thinner line contours correspond to high- and low-shear velocity perturbations, respectively. Velocity contour intervals are 0.5% and $|\delta V_S| \geq 0.5\%$ (i.e., the zero value contour is not drawn). Shear wave anisotropy or discontinuity analyses conducted in the highlighted areas, according to region are: (1) Mitchell and Helmberger (1973), Lay and Helmberger (1983a,b), Zhang and Lay (1984), Kendall and Shearer (1994), Kendall and Nangini (1996); Kendall and Silver (1996, 1998) and Ding and Helmberger (1997); (2) Lay and Helmberger (1983a), Young and Lay (1990), Weber and Davis (1990), Lay and Young (1991), Kendall and Shearer (1994), Matzel et al. (1996) and Garnero and Lay (1997); (3) Weber and Davis (1990), Gaherty and Lay (1992), Kendall and Shearer (1994), Valenzuela and Wysession (1998) and Thomas and Kendall (2002); (4) Young and Lay (1990), Ritsema (2000); (5) Vinnik et al. (1989, 1995, 1998), Garnero et al. (1993), Pulliam and Sen (1998), Valenzuela and Wysession (1998), Ritsema et al. (1998), Russell et al. (1999, 2000, 2001), Fouch et al. (2001). Region (5) is distinct in that it coincides with large scale low-shear velocities.

Several studies have presented evidence for a D″ shear velocity discontinuity several hundred kilometers above the CMB in our study region (Lay and Helmberger, 1983a,b; Zhang and Lay, 1984; Kendall and Shearer, 1994; Kendall and Nangini, 1996; Ding and Helmberger, 1997). For a more comprehensive listing of D″ discontinuities detected globally, see the review by Wysession et al. (1998). While 1D radial profiles have been shown to fit the average *S-Scd-ScS* waveform behavior of the data (e.g., Lay and Helmberger, 1983a; Ding and Helmberger, 1997), evidence for significant lateral variations across the region exists. Kendall and Nangini (1996) model discontinuity depths as 250–290 km above the CMB, with no clear evidence for a discontinuity in a localized region in the center of our study area. Kendall and Shearer (1994) infer a variable thickness of the D″ layer below the discontinuity of 150–200 km just west of Panama, and ∼300 km to the east. Ding and Helmberger (1997) used travel time and waveform modeling to define a D″ discontinuity 200 km above the CMB west of Central America.

On a global basis, there have been many aspects of the D″ discontinuity structure addressed in past studies. These include: possible existence of a negative velocity gradient below the velocity jump (e.g., see Young and Lay, 1987); the sharpness of the velocity increase, which may be gradational over up to 50–70 km depth extent (Young and Lay, 1987; Garnero et al., 1993); and also the height of the D″ discontinuity above the CMB, which can trade-off with structure above and below the discontinuity, as well as discontinuity strength. In this paper, we do not attempt to resolve these issues, as our intent is to develop a general relationship between the existence of the discontinuity and other attributes of the D″ structure. We therefore identify the regions that produce a reflection (*Scd*) from D″ apparent in the individual waveforms. A comparable analysis of *P* waves cannot be done, due to the obscuring effects of *P* wave coda, which must be suppressed by stacking (e.g., Reasoner and Revenaugh, 1999). Many hypotheses have been put forth for the origin of the D″ discontinuity. These include a chemically distinct layer, slab related thermal anomalies, a phase change, or a rheological fabric change (e.g., see reviews or investigations by Matzel et al., 1996; Wysession, 1996; Wysession et al., 1998; Sidorin et al., 1999; McNamara et al., 2001, 2002). In this paper, we demonstrate that any explanation for the D″ discontinuity in our region must be consistent with the feature having lateral dimensions of well over 1000 km.

Shear wave splitting of the radially polarized *SKS* phase is routinely used for studies of upper mantle anisotropy (e.g., see reviews by Silver, 1996; Savage, 1999). Similarly, for shear waves traversing the deepest mantle, namely *ScS*, *S*, and diffracted $S(S_{\mathrm{diff}})$, splitting has been documented for nearly 30 years. Mitchell and Helmberger (1973) observed *ScS* arrivals offset in time between the radial and transverse components of motion. A decade later, Lay and Helmberger (1983b) showed similar observations in their analyses of shear wave discontinuity structure in the lowermost few hundred km of the mantle. Many studies have subsequently presented evidence for shear wave splitting of deep mantle phases, inferring lowermost mantle anisotropy (e.g., see Vinnik et al., 1989, 1995, 1998; Lay et al., 1991, 1998a,b; Montagner, 1998; Kendall, 2000). Kendall and Silver (1996, 1998) have presented clear evidence for D″ anisotropy in our study area.

Locations sampled in previous studies of D″ anisotropy are shown in Fig. 1. Nearly, all of these regions have also been investigated for D″ discontinuity and shear velocity heterogeneity structure. Deep mantle anisotropy has been inferred in both high velocity (regions 1–4, Fig. 1) and low velocity (region 5, Fig. 1) regions of D″. Anisotropy is commonly used to infer aspects of mantle dynamics such as a subduction-related origin in circum-Pacific regions (e.g., Kendall and Silver, 1996; McNamara et al., 2002) and plume-related origin in the central Pacific (e.g., Russell et al., 1998, 1999; Fouch et al., 2001; Romanowicz and Gung, 2002).

The transition in depth from an isotropic lower mantle to an underlying anisotropic D″ structure, if abrupt, may be the cause of the D″ discontinuity (Matzel et al., 1996; Lay et al., 1998a,b). Similarly, D″ has been speculated to be a zone of increased heterogeneity that may result in the onset of anisotropy due to shearing in the boundary layer, which could also give rise to *Scd* arrivals (Cormier, 2000).

While many possibilities exist for the origin of D″ anisotropy that involve either lattice preferred orientation (LPO), or shape preferred orientation

(SPO) this remains a very speculative topic, with little experimental foundation and great difficulties for uniquely characterizing the anisotropic geometry. We refer the reader to several studies that discuss mechanisms that may give rise to D″ anisotropy (e.g., Karato, 1993; Karato, 1998; Karki et al., 1999; Kendall, 2000; Mainprice et al., 2000; Yamazaki and Karato, 2002; McNamara et al., 2002). Our focus in this paper is on mapping the geographic trends in the shear wave splitting across our study area, inferring anisotropy strength from this splitting, and then making geographic comparisons of inferred anisotropy, heterogeneity, and the D″ discontinuity. Most of our data are compatible with VTI (simple delays of *SV* relative to *SH*), but in detail we believe some observations do require azimuthal anisotropy, perhaps as a mild deviation from a purely vertical hexagonal symmetry axis. The first-order splitting effect can still be reliably measured, and future work will delve into the details of the deviations from VTI in the region.

South American earthquakes recorded in North America offer an opportunity to jointly investigate D″ shear velocity heterogeneity, anisotropy, and D″ discontinuity structure by providing a large epicentral distance range due to an extended north–south trench system containing suitable intermediate and deep focus earthquakes, and the numerous recording networks in North America. In this study, we investigate D″ beneath the Caribbean and Central America through study of shear velocity heterogeneity (from differential times of *S*-*SKS* and *ScS*-*S*), anisotropy (from shear wave splitting of *ScS*, *S*, and S_{diff}), and D″ discontinuity (from detection of *Scd*). In the following sections, we demonstrate that the base of the mantle in our study area is predominantly seismically high velocity, with the highest velocities to the west, and that mid-mantle heterogeneity plays an important role in affecting *ScS*-*S* times. Strong variations in heterogeneity and anisotropy are prevalent throughout our study area, with a suggestion of heterogeneity and anisotropy strength being coupled. We observe systematic variations in the presence and disappearance of *Scd* at small geographic scales. In addition to developing a cohesive view of these first-order observations, we also identify key localized areas for future research that will help to resolve many important issues raised.

2. South American earthquake data set

A combined North American World-Wide Standardized Seismographic Network (WWSSN) and broadband station shear wave database is utilized for this study. Long-period WWSSN data from South American deep focus earthquakes digitized by Lay (1983); Lay and Helmberger (1983a,b), and Kuo et al. (2000) are used; along with broadband data from the Incorporated Research Institutions for Seismology (IRIS), the Canadian National Seismic Network (CNSN) and the United States National Seismographic Network (USNSN) (see Table 1). Data are selected based on good signal-to-noise ratio and relatively simple source processes for earthquakes deep enough to separate surface-reflected phases from the down-going phases of interest. These criteria restrict us to earthquake magnitudes in the range 5.5–6.9 and source depths from 100 to 650 km.

The following measurements were made: (a) differential arrival times between transverse component *S* (or S_{diff}) and longitudinal component *SKS*; (b) differential arrival times between transverse components of *ScS* and *S*; (c) splitting times between the transverse and vertically polarized components of *ScS* (*ScSH* and *ScSV*, respectively); (d) splitting times between the *SH* and *SV* components of *S* or S_{diff}; and (e) identification

Table 1
Number of data measurements

Structure	Measurement	Data[a]	Number of observations
Heterogeneity	δT_S (*S*-*SKS*)	WW	106
		BB	163
		LP	59
	δT_S (*ScS*-*S*)	WW	111
		BB	159
		LP	30
Anisotropy	*SV*-*SH*(S_{diff})	WW	38
		BB	74
		LP	13
	SV-*SH*(*ScS*)	WW	62
		BB	52
		LP	6
D″ Discontinuity	*Scd* ID	WW	99
		BB	198

[a] WW: WWSSN data; BB: broadband data; LP: broadband data low pass filtered at 10 s.

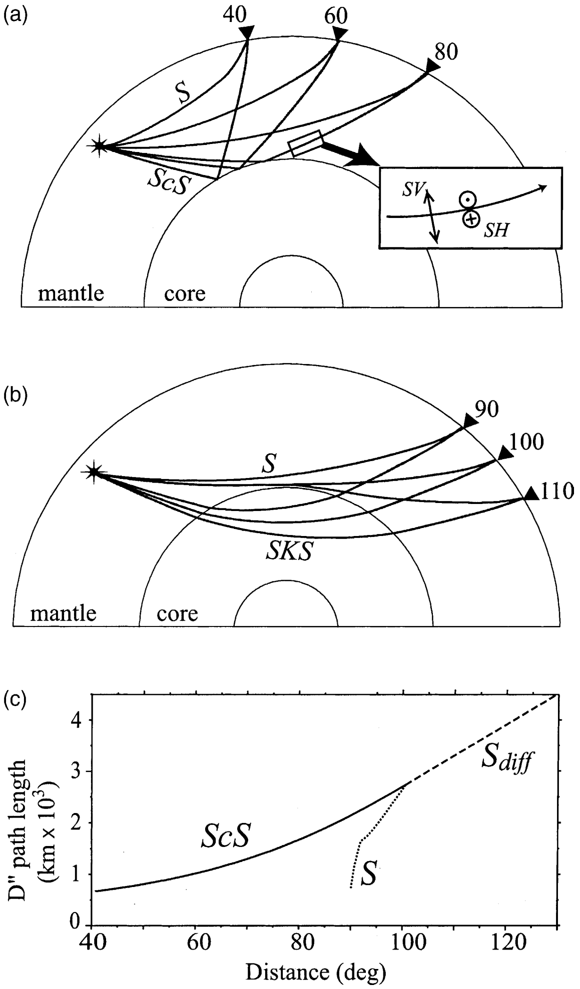

Fig. 2. Ray path geometry of (a) *S* and *ScS* waves, and (b) *S* and *SKS* waves. The inset in panel (a) depicts the orthogonal particle motion directions of *SH* and *SV*. (c) Length of *ScS*, *S*, and S_{diff} in a 250 km thick D″ layer, as predicted by the PREM model.

of the presence or absence of the *Scd* arrival between *S* and *ScS* due to triplication from a high-velocity zone in D″. Fig. 2 shows ray path characteristics of the *ScS*-*S* and *S*-*SKS* data sets (*S*-*SKS* denotes either *S* or S_{diff} minus *SKS*). Differential times are used because they minimize contributions from upper mantle heterogeneity, since their paths are quite similar there, as well as reducing effects of source mislocation and origin time errors. As Fig. 2c illustrates, the path lengths within D″ can be significant for these phases, especially for S_{diff}. The *ScS*-*S* and *S*-*SKS* differential times are especially sensitive to velocity structure in the deep mantle.

The ray path coverage of our *ScS*-*S* and *S*-*SKS* data sets is shown in Fig. 3. We focus this study on the lower mantle region beneath the Caribbean and Central America where the path coverage is abundant. In the western portion of our study area, the ray path coverage for the *S* and *ScS* waves is particularly dense. To better display the data coverage, ray density within D″ is calculated for $1^\circ \times 1^\circ$ cells, using the PREM model (Dziewonski and Anderson, 1981) for all ray path geometry predictions (Fig. 3c). This path coverage density far surpasses previous studies, but suffers (as with most deep mantle investigations) from almost nonexistent crossing ray path coverage. Thus we expect that our inferred patterns of heterogeneity may be smeared in the north-south direction along the ray paths. We note that systematic errors due to using a simple reference model like PREM for a region that may contain a D″ discontinuity should not significantly affect these ray density computations, although turning depths may be in error by as much as several hundred kilometers for *S* phases at triplication distances.

All broadband data discussed below have been deconvolved by the instrument response to obtain ground displacements, then bandpass-filtered between 1 and 100 s. Upper mantle anisotropy corrections based on published studies of lithospheric anisotropy (e.g., see Silver, 1996) are applied to all data prior to rotation to the great-circle reference frame. That is, all phases are rotated into a fast/slow polarization reference frame, reverse time-shifted by some splitting time, then rotated to great-circle components. This is particularly important for broadband data, given that these corrections can involve up to 2.5 s of splitting between fast and slow polarizations. We note that these lithospheric corrections are often based on limited azimuthal and ray-parameter sampling of the receivers, and their predictive value for diverse phases with a range of azimuths and incidence angles is limited. We often observe that the corrections actually increase either the non-linearity of shear wave particle motion or fail to eliminate the *SKS* energy on the transverse component (as discussed in Garnero and Lay, 1997), but this is the best that can be done given current understanding of the lithosphere. Another uncertainty relates to differing arrival angles of S_{diff}, *S*, or *ScS* at seismic stations,

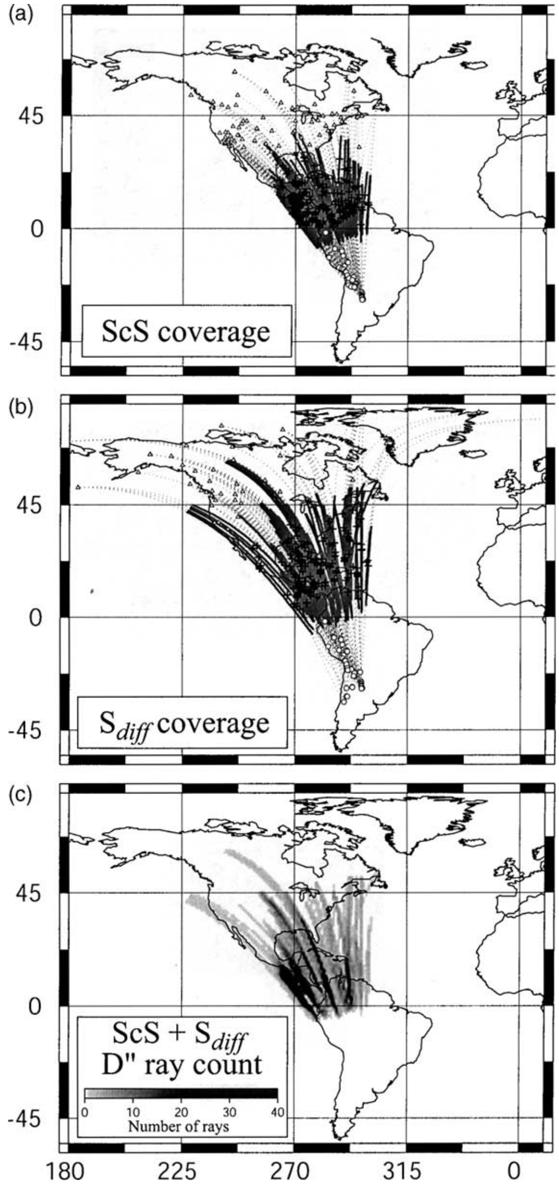

Fig. 3. (a) South American earthquakes (open circles), seismographic stations (open triangles), great circle path geometry for *ScS* data (dotted lines), PREM-predicted path coverage in a 250 km thick D″ (thick gray lines), and CMB midpoints of paths (crosses). (b) Same as (a), except for *S* or $S_{\rm diff}$. (c) Ray sampling of D″. *ScS* and $S_{\rm diff}$ rays are counted in $1^\circ \times 1^\circ$ cells. The south and western portion of our study area contains the highest ray coverage density.

especially when most available upper mantle lithospheric anisotropy corrections are derived using *SKS* waves. *ScS* should have incident angles much closer to *SKS* than do Sdiff, thus a slight mis-correction for $S_{\rm diff}$ can occur. Therefore, any inferences made about D″ anisotropy must emphasize regionally coherent patterns that are unlikely to be the result of bias in the individual lithospheric corrections.

Fig. 4 shows representative broadband shear waveform data for the November 28, 1997 deep focus event (source depth = 586 km). Fig. 4a displays a distance profile for broadband *S* and *ScS* transverse component displacement data. Both the *S* and *ScS* arrivals are clear and impulsive. Accurate differential arrival times can be measured from these seismograms. For the same event, Fig. 4b shows five pairs of longitudinal *SV* and transverse *SH* recordings containing *SKS* and *S*. Arrival onsets are typically strong and impulsive. The receiver anisotropy corrections should reduce any effects of comparing longitudinal *SKS* and transverse *SH* component arrival times. Readily visible delays of *S* phases on the *SV* components relative to the *SH* components are indicated.

Our broadband data set is augmented by two additional data sets: (1) low-pass filtered versions of all of the broadband data, with a corner period of 10 s. This filtering enables use of some data that would otherwise have too low signal-to-noise ratios; this densifies our D″ path coverage. Measurements from the low-passed (LP) data compare well to the raw broadband (BB) data measurements for observations with good signal-to-noise ratios. Hence we expect no significant contamination of the LP measurements due to frequency dependence of travel time measurements. It appears that the reduced temporal resolution of the filtered traces is compensated by the improved coherence of the waveforms, yielding stable relative arrival time measurements. (2) Long-period World-Wide Seismographic Station Network (WW) data. These analog data have been digitized and rotated into great-circle path geometries, but are not deconvolved to ground motion. These data greatly augment path coverage of our study area, since they provide different station locations from the modern digital networks. We have very limited information about anisotropy corrections for the WWSSN stations, but the long-period signals tend to have only minor modifications when corrections are applied (and note that anisotropy corrections

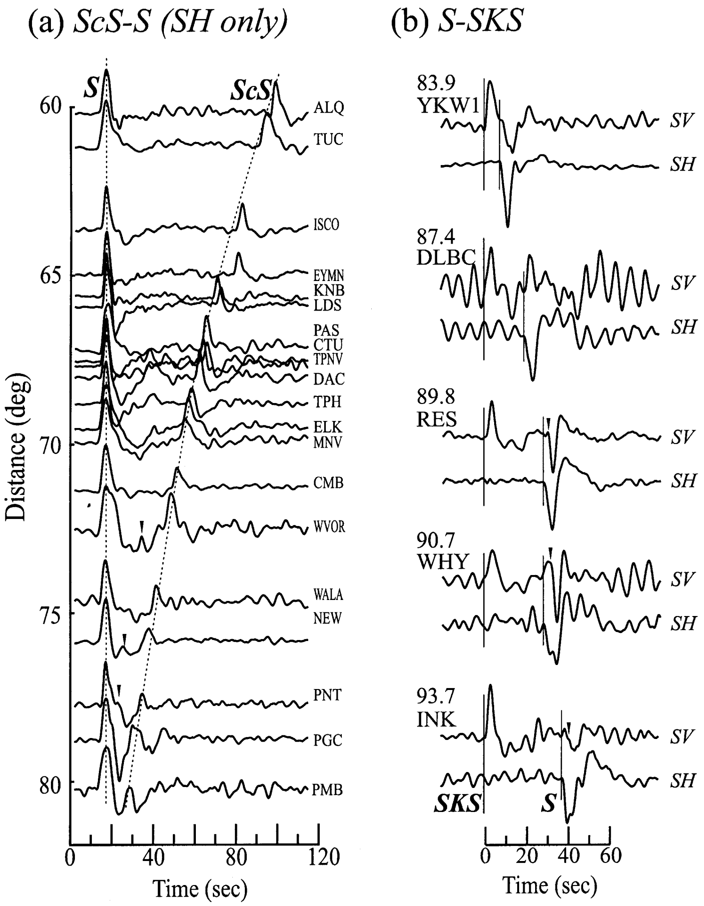

Fig. 4. Broadband displacement waveforms for deep focus South American event of 11/28/97. (a) Tangential component *S* and *ScS* data are shown, normalized in time and amplitude to the direct *S*. The *ScS* arrival is clear and impulsive, with some evidence for a intermediate arrival (inverted black triangles), the *Scd* phase. (b) Pairs of *SV* and *SH* traces for the *SKS* through *S* time window for five stations. Some data display a delay in the *SV* component *S* waves (inverted black triangles). Each of these delays is ∼2 s.

may have a significant frequency dependence, e.g., see Silver and Chan, 1988). We find very good consistency between broadband and WWSSN measurements in regions of common ray geometry.

3. D″ heterogeneity inferred from differential travel times

3.1. Differential travel time residuals

Differential travel times were measured for *ScS-S* and *S-SKS* data. *ScS-S* times were measured by peak-to-peak times on the transverse component of motion. The peak-to-peak measurement was chosen since *S* and *ScS* are typically similar in frequency content, and the onset time of *ScS* is often ambiguous due to *S* wave coda. We estimate the accuracy of the *ScS-S* differential times to be on the order of ±0.5 s. *S-SKS* times were computed from the difference between S_{SH} and SKS_{SV} onset times. For these phases, peak-to-peak times are less reliable owing to the frequency content differences common to *SKS* and *S*, while the onsets are relatively clear because these are first arrivals on their respective components (there can be mild contamination from *SKSp* crustal conversions, but this is weak on the radial components). When picks of the broadband data were questionable, we checked the results relative to the LP versions to assess the quality. Our measurement accuracy for *S-SKS* differential times is conservatively estimated to be within ±1 s. We chose not to use a cross-correlation scheme to measure relative timing between data and synthetic seismogram predictions, primarily due to broadband waveform variability (especially for *SV*) in the diffracted and reflected waves (this is apparent in Fig. 4). Differential travel time residuals were computed relative to the 1 s PREM model (observed differential time minus predicted). *ScS-S* and *S-SKS* travel time residuals are noted as $\delta T_{ScS\text{-}S}$ and $\delta T_{S\text{-}SKS}$, respectively. All travel time residuals then were corrected for the aspherical structure of Grand (2002) as follows: aspherical model predictions for *ScS* and *S* paths above a 250 km thick D″ layer were removed from $\delta T_{ScS\text{-}S}$. The $\delta T_{S\text{-}SKS}$ residuals were corrected for aspherical predictions for *SKS* for the entire mantle, and for *S* raypaths above the 250 km thick D″ layer (motivated by the fact that most of our SKS paths traverses D″ to the north or south of our focused study area). Thus, hereafter, $\delta T_{ScS\text{-}S}$ and $\delta T_{S\text{-}SKS}$ denote residuals corrected for Grand's relatively high-spatial resolution model of mantle asphericity apart from the portions of raypaths turning in the 250 km thick D″ layer.

The choice of model used for removing shallow contributions from measured residuals affects the corrected residuals; tomographic models vary in spatial resolution and strength of heterogeneity. We use the recent model of Grand (2002), a block model with lower mantle horizontal elements that are roughly 250 km^2, because it has relatively high-spatial resolution and this model incorporated extensive data coverage in our study region. This choice of model is subjective, but we note the high degree of similarity between this model and that of Ritsema and Van Heijst (2000), another relatively high-resolution recent tomographic model.

Differential travel time residuals of $\delta T_{ScS\text{-}S}$ and $\delta T_{S\text{-}SKS}$ are shown as functions of propagation distance in Fig. 5a and b. The raw residuals are plotted as crosses, and circles represent residuals corrected for mantle asphericity. A primary characteristic of these data is that the residuals are predominantly negative. This is consistent with early *ScS* arrivals in the *ScS-S* pairs, or early S_{diff} arrivals in the S_{diff}-*SKS* pairs—each resulting in a diminished differential time that yields a negative residual. Invoking the alternate possibility of late *SKS* arrivals or late *S* arrivals for the two differential time data sets (S_{diff}-*SKS* and *ScS-S*, respectively) runs contrary to all models of mantle structure in the vicinity. In what follows, we attribute these negative residuals to the presence of high-shear velocities in D″ (relative to PREM velocities) that speed up arrivals with paths in D″. Table 1 summarizes the number of data used. Also shown in Fig. 5a and b is a prediction for a 1D shear velocity model of Kendall and Nangini (1996), SKNA2. This model contains a first-order D″ shear velocity discontinuity of about 2.5% 290 km above the CMB with the shallower structure being very close to PREM. The general agreement between the SKNA2 predictions and both sets of travel time anomalies indicate that high-shear velocity in D″ is widespread across our study area. The large scatter about the SKNA2 predictions, which greatly exceeds the measurement error, does suggest the additional presence of strong small-scale heterogeneity in the region. Correcting the residuals for non-D″ mantle heterogeneity does not significantly alter the $\delta T_{S\text{-}SKS}$ times (Fig. 5a). $\delta T_{ScS\text{-}S}$ times, however, involve *S* waves that bottom in the mid-lower mantle, a depth range containing significant shear velocity heterogeneity beneath the Caribbean (e.g., Grand et al., 1997). Thus, the corrected $\delta T_{ScS\text{-}S}$ residuals show significantly reduced scatter compared to the raw residuals, including elimination of almost all positive anomalies (Fig. 5b). The corrected residuals in Fig. 5a and b are used to infer geographic patterns of D″ heterogeneity in the rest of this paper.

The PREM-predicted ray path bottoming depths relative to the CMB as a function of propagation distance are indicated in Fig. 5a for a 500 km deep source. (Note: these lines will shift ∼2° to the right for a 100 km deep source). Here we see the predominance of reduced *S-SKS* times (relative to PREM) for the bulk of our data traversing the deepest mantle. Some of the data suggest significant heterogeneity at least up to 300–350 km above the CMB, but the baseline for these data is close to PREM. Data with PREM-predicted bottoming depths above a 250 km thick D″ are not used for our D″ analyses. If there is a high-velocity layer in D″ that causes a triplication of *S*, the bottoming depths for data less than 90° away may be significantly deeper than predicted for the PREM model. For example, as indicated by Lay et al. (1997), rapid fluctu-

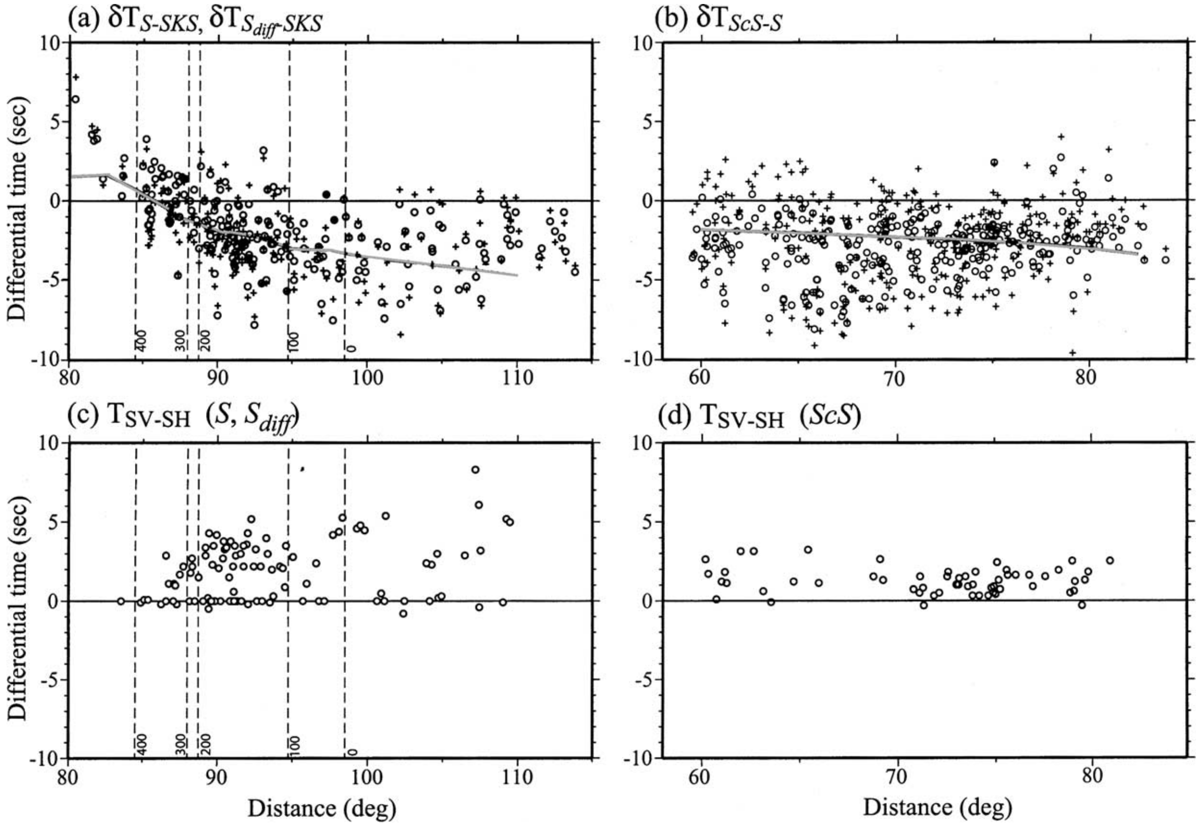

Fig. 5. (a) S_{diff}-*SKS* and (b) *ScS-S* differential travel time residuals, as measured relative to the PREM model. Both differential travel times are consistent with a high-velocity lower mantle structure, as indicated by the prediction of shear wave discontinuity model SKNA (Kendall and Nangini, 1996) (thick gray line). Raw residuals are displayed as crosses; those corrected for non-D″ heterogeneity (of Grand, 2002) are shown as open circles. The lower two panels present shear wave splitting measurements of (c) *S* or S_{diff} and (d) *ScS*. Also shown in panels (a) and (c) are distances associated with PREM-predicted ray path bottoming depths for a 500 km deep source.

ations in *ScS-Scd* differential times indicate that travel time anomalies likely accumulate within a relatively thin zone toward the top of D″. Accurate knowledge of structure is needed to predict the ray path geometries for precisely estimating the amplitude of heterogeneity. Our cutoff of PREM-predicted bottoming depth of 250 km above the CMB is conservative; surely all data satisfying this are in fact bottoming within the D″ layer given that it is higher velocity than in PREM, and we will have little error in estimating the total path length within the D″ region for corresponding phases.

3.2. Inferred D″ heterogeneity

To provide a first-order estimation of volumetric heterogeneity in our study area, we employ the simple method of: (a) estimating D″ seismic wave path lengths, using PREM; (b) using a D″ reference velocity, again from PREM, and the travel time anomaly to infer the uniformly distributed velocity anomaly along the D″ path for each differential time. Fig. 6 shows the resulting estimates of shear velocity heterogeneity from our $\delta T_{ScS\text{-}S}$ and $\delta T_{S\text{-}SKS}$ residuals. In panel (a), the raw velocity heterogeneity estimates are plotted at the location of the CMB path midpoints. The largest δV_{S} estimates (for the uncorrected residuals) in our study area are up to +6%, the lowest are −2%. The magnitude of these estimates will shift for different reference models, but the relative patterns are expected to be quite robust.

Fig. 6b displays the corresponding residuals after correcting for non-D″ mantle heterogeneity using the

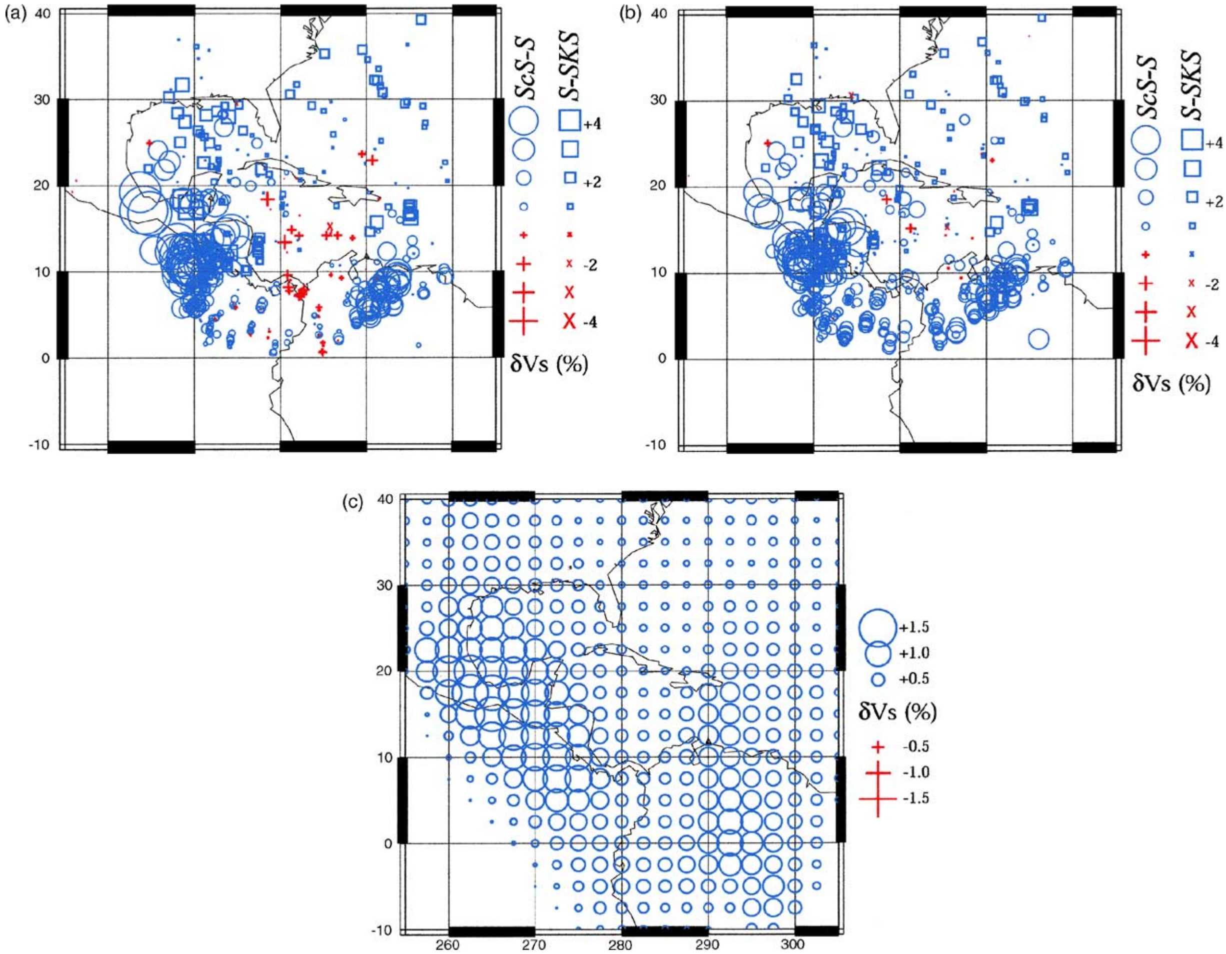

Fig. 6. (a) Shear wave heterogeneity estimations from raw $\delta T_{ScS\text{-}S}$ (circles and crosses) and $\delta T_{S\text{-}SKS}$ (squares and X's) residuals for a 250 km thick D″ layer. Blue and red colors correspond to high and low velocities, respectively, and are plotted at the CMB bounce (or mid-) points of *ScS* or *S*. (b) Same as (a), except residuals have been corrected for non-D″ aspherical structure of Grand (2002). (c) Gaussian cap-averaging of heterogeneity estimates of (b) distributed along PREM-predicted D″ paths. The smoothing results in all velocities being fast.

Grand (2002) model. After correction, the extrema of the dataset have reduced by ∼1%, that is, nearly all predicted heterogeneity falls in the range between −1 and +5%. Coherent spatial patterns of heterogeneity are seen in the δV_S map of Fig. 6b. The largest residuals are grouped in an area beneath Central America (and slightly to the west), and high velocities are also seen under northernmost South American beneath Venezuela. High velocities are prevalent throughout the rest of our area, but diminish to the northeast around a longitude of 285°. Shear wave heterogeneity inferred from the *ScS*-*S* data set is ompatible with that from *S*-*SKS* data (Fig. 6a and b).

We note that $\delta T_{S\text{-}SKS}$ can be affect by perturbations in the *SKS*(SV) leg through an anisotropic D″. However, this is difficult to assess since the geometry of anisotropy within D″ is not well constrained. Our assumption in this paper is that *SKS* is a relatively stable reference time, since its D″ path length is significantly shorter than that of S_{diff}. The consistency in heterogeneity estimates of D″ heterogeneity from *ScS*-*S* and *S*-*SKS* times suggests validity in this assumption.

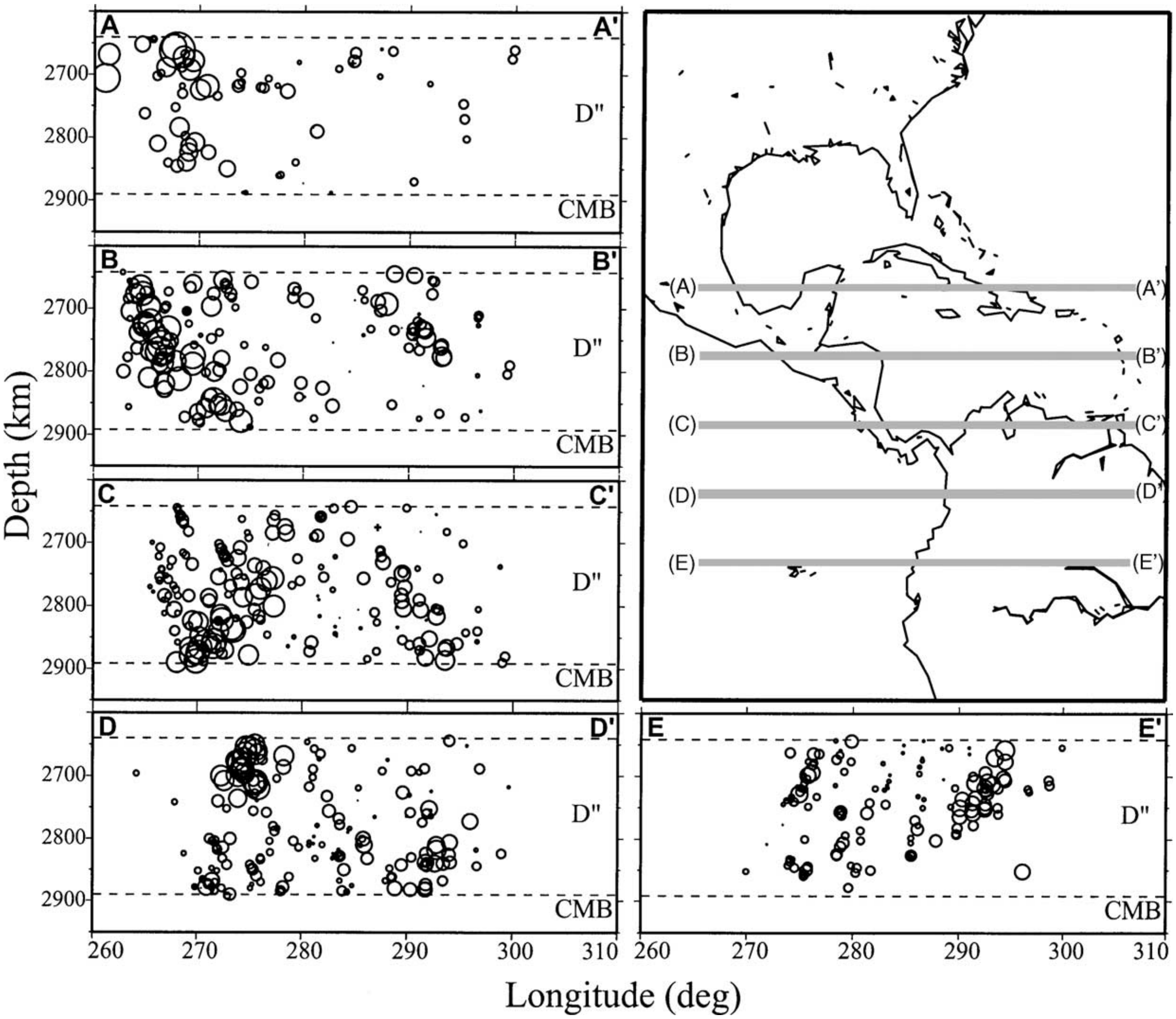

Fig. 7. Map in the upper right displays five west-to-east cross-section lines, which are shown in a counter clockwise fashion from AA′ to EE′. The cross-sections display the bottom 250 km of the mantle. Symbols in each cross-section represent a δV_S heterogeneity estimate plotted where the *S* or *ScS* raypaths pierce the plane of the cross-section. Plotted δV_S correspond to *ScS-S* and *S-SKS* residuals corrected for non-D″ heterogeneity (of Grand, 2002). The largest symbols correspond to ∼5% fast, relative to PREM.

Plotting residuals at the mid-point of the D″ ray segment fails to account for the finite path length over which the anomalies are assumed to accumulate. The δV_S estimates of Fig. 6b were therefore spread along the D″ portion of all *S*, S_{diff}, and *ScS* ray paths and smoothed with a floating Gaussian cap. A 5° radius Gaussian cap was computed at each node of a 1° × 1° grid. The resulting δV_S distribution is displayed in Fig. 6c. This is a somewhat more realistic portrayal of the region sampled by our data, although it is likely that small-scale strong lateral gradients are excessively smoothed out. First-order results are that the highest velocities are beneath Central America and Mexico while the Caribbean is underlain by only moderately fast material. While some streaking along ray paths is apparent, the smoothed representation of heterogeneity highlights the two high-velocity regions discussed above.

Another portrayal of the inferred heterogeneity distribution is shown in five east-west cross-sections

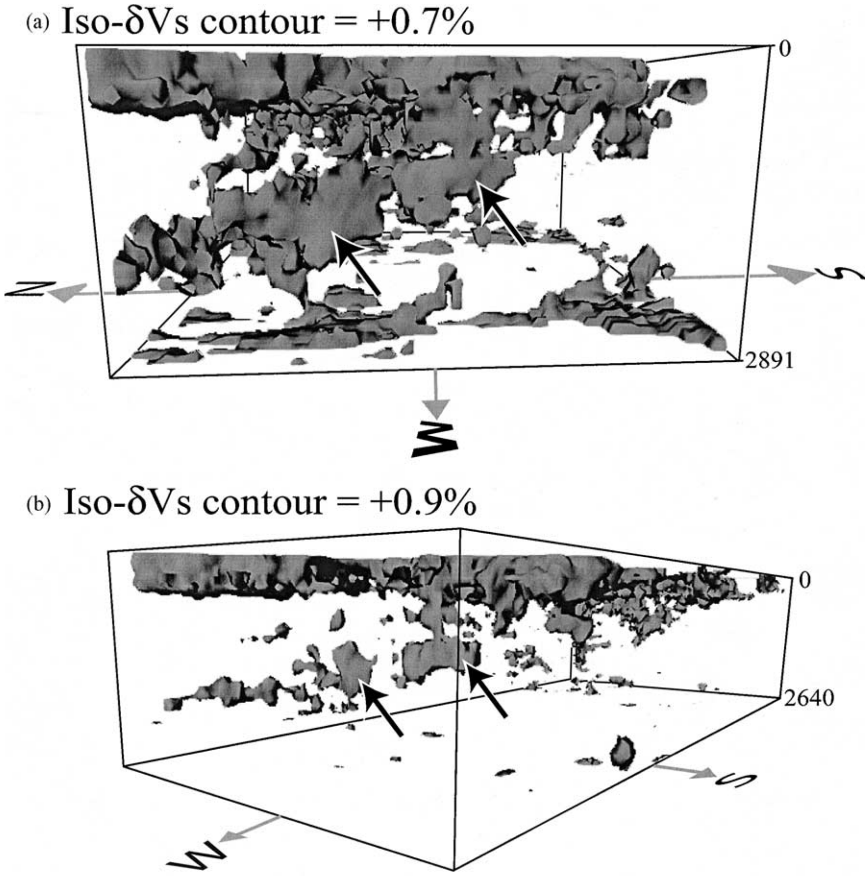

Fig. 8. (a) Iso-velocity contouring of high velocities in the Grand (2002) model in the mantle beneath Central and South America, viewing mantle structure from crust to the CMB from the west. The contour is set at 0.7%, thus any contoured shape contains shear velocities at or greater than 0.7%. The arrows indicate two large tabular features in the mid-lower mantle, likely remnant Farallon slab material. (a) Same as (a), except depth range excludes D″, and velocity cut-off contour is now 0.9%.

through D″ in Fig. 7. Heterogeneity estimates are plotted at the ray path piercing points to each cross-section. Small-scale coherent patterns are apparent, such as: higher velocity concentration towards the top of D″ in cross-sections A and D (to the west), high velocities throughout the western part of B, and only mild high velocities in E. In general, the western part of the cross-sections possesses the highest wave speed estimates.

3.3. Mid-mantle contamination of ScS-S times

The differences between Fig. 6a and b reflect the importance of correction for mantle heterogeneity above D″ in this region. Mid-mantle anomalies have been identified previously in this region, using the same WWSSN records as we have used here: Lay (1983) identified mid-mantle anomalies from *ScS*-*S* times with scale length 1000–2000 km, and strength $\sim$+2% for both *P* and *S* waves (see also Jordan and Lynn, 1974; and Bokelmann and Silver, 1993). This is in excellent agreement with the δV_S model of Grand (2002). Fig. 8 shows the Grand (2002) model with two different volumetric renderings of iso-velocity contours for velocities that are above 0.7% fast. This figure has a viewpoint looking east from west of South and Central America. The arrows in Fig. 8 denote two significant mid-mantle high-velocity anomalies, which are commonly interpreted as corresponding to the ancient Farallon slab discussed in Grand et al.

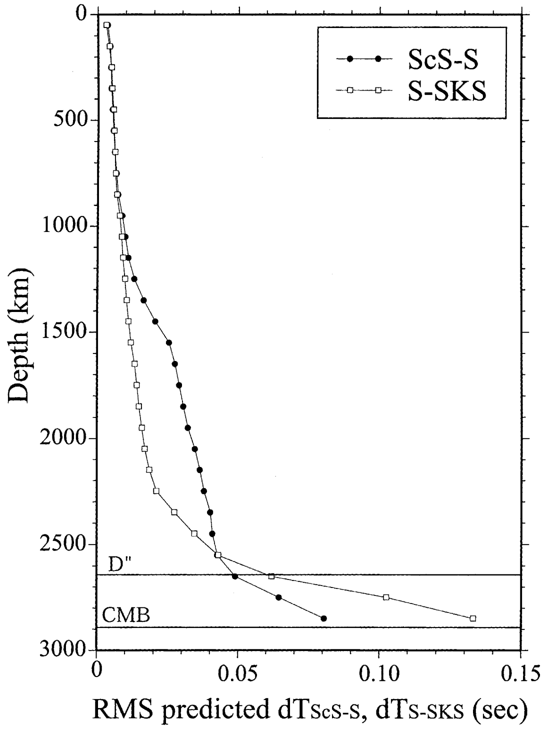

Fig. 9. *ScS-S* and *S-SKS* differential times have been predicted from the Grand (2002) mantle model for the exact wave path geometries of our data set. The predicted contributions to these differential times in every 100 km depth shell of the mantle was computed, and the RMS of these contributes are shown separately for the *ScS-S* and *S-SKS* residuals. The *ScS-S* data are affected by mantle structure as high up as 1500 km above the CMB (see text for details).

(1997). This heterogeneity persists even for the >0.9% level (Fig. 8b), and coincides with the mantle paths of many of our *S* arrivals in the *ScS-S* pairs.

These mid-mantle anomalies can contribute significantly to the *ScS-S* differential travel times because the tabular features are oriented along the earthquake-station *S* ray paths. To quantify the magnitude of predicted travel time contributions of heterogeneity at different depths in the mantle, cumulative travel time anomalies are estimated for our data paths from 100 km depth shells throughout the mantle model of Grand (2002). The RMS averages of these predictions are shown separately for *S-SKS* and *ScS-S* times in Fig. 9. As expected, the contributions to *S-SKS* are largest at the base of the mantle, where *S* waves bottom, and have significant horizontal propagation length in the high-velocity D″ region of the model (see Fig. 2c). *ScS-S* residuals show significant contribution from the mid-mantle, starting at ∼1500 km depth, increasing as the *ScS* paths graze through D″.

While the Grand (2002) model must have limited predictive accuracy, application of the mantle corrections outside of D″ does reduce the range of residuals, along with enhancing spatial coherence of the anomalies. Our results do not reveal the low-velocity D″ feature imaged in Wysession et al. (2001); Tkalcic and Romanowicz (2001), and Fisher et al. (2003) under northern South America (latitudes 8–10°, longitude 280–290°) after correcting for the Grand (2002) structure. While the raw data do have some negative differential times for paths under the Caribbean and Colombia that could suggest the presence of such a feature, after allowing for the finite path length of *ScS* in the D″ layer (Fig. 6a), the model corrections reverse the sign of most of these anomalies (Fig. 6b), leaving slightly fast average structure under the Caribbean and under Colombia. We note that our path coverage is not as dense as these recent regional efforts, thus we do not have the acute resolving power of a their localized region. There is no question that higher resolution sampling of D″ should reveal many features that our larger-scale study fails to resolve.

4. D″ anisotropy inferred from shear wave splitting

4.1. Shear wave splitting measurements

Splitting between the *SH* and *SV* components of *ScS* waves was measured between the *ScS* peaks, effectively assuming that any shift of the peaks is due to VTI. *S* (or *Sdiff*) splitting was measured between the onsets of *S* (or $S_{\rm diff}$) on the *SH* and *SV* components. While there can be up to a ±1 s error in splitting estimates for the onset time method for noisy data, we adopted this approach rather than any particular cross-correlation scheme due to significant $SV_{\rm diff}$ waveform variability. Fig. 4b displays the nonuniformity of $SV_{\rm diff}$ pulses for an event with fairly clean data. Important requirements for any earthquake to be used for splitting analysis are the need for strong *SV* and *SH* radiation, good signal-to-noise ratio, and a simple source time function. While requirements are difficult to satisfy for some source-receiver geometries, the wave path corridor used here produces ample data with these attributes (Table 1). Fig. 5c and d show the *S* (or *Sdiff*) and *ScS* splits for our study region as functions of epicentral distance. As demonstrated in previous studies (e.g., Kendall and Silver, 1996), the maximum S_{diff} splits appear to grow with epicentral distance as D″ paths increase in length. Note that almost all of the splitting measurements are zero or positive (delayed *SV* peaks/arrivals). This is compatible with the expectation of VTI; transverse components will always arrive earlier for this form of anisotropy. Note, however, that this is not a unique demonstration that the geometry must be VTI; seldom are the phase onsets so clear that some level of coupling between the *SH* and *SV* signals (as would arise from azimuthal anisotropy) can be absolutely precluded. It is also possible that azimuthal anisotropy could lead to systematic delays of *ScSV* peaks relative to *ScSH* peaks. However, the data are remarkably consistent allowing for the uncertainties of the lithospheric corrections. Overall, we can state that the observations are at least compatible with laterally varying magnitude of VTI throughout the region.

4.2. Inferring D″ anisotropy

Our approach to inferring anisotropy strength is essentially the same as that for velocity heterogeneity. The splitting times (from Fig. 5c and d) are used along with D″ path length estimates from the PREM model, for a 250 km thick layer, and PREM velocity structure to estimate the uniform D″ path average anisotropy. As with the heterogeneity estimates, the strength of inferred anisotropy depends on the assumed thickness of D″. Our choice of 250 km was motivated to correlate with the thickness of the deepest layer in the Grand (2002) structure. This thickness is also intermediate to estimates of the height above the CMB of a D″ shear velocity discontinuity, which range from 200 to 350 km (Lay and Helmberger, 1983a; Kendall and Nangini, 1996; Ding and Helmberger, 1997). In two other regions, Fouch et al. (2001) chose a D″ thickness based on the onset of negative velocity gradients. While any choice is essentially subjective given the lack of vertical resolution, the patterns of anisotropy heterogeneity will not significantly change. Rather, the amplitude of patterns will increase or decrease. Since our purpose is to map the gross trends of anisotropy over our entire study region, we will not pursue this dependency on assumed D″ thickness any further here. Better data coverage throughout the region would be necessary to map the depth extent of anisotropy in D″, which we leave for future efforts.

Several uncertainties exist in seismic modeling of D″ anisotropy. Garnero and Lay (1998) demonstrated the limitations of using observed splitting times and simple ray tracing to calculate anisotropy over an assumed D″ depth range. Also, recent synthetic calculations demonstrate the existence of strong waveform and splitting time dependence on the structural details of any model (Moore et al., 2003). Structural features such as D″ discontinuity existence, anisotropy depth distribution, velocity gradient above or below anisotropic structure, and geometry of anisotropy, are all important factors contributing to different waveforms and splitting times. These complexities are beyond the scope of our current mapping of gross patterns in D″ anisotropy for this region.

The geographic pattern of inferred anisotropy for our data set is displayed in Fig. 10a at the CMB midpoints. Anisotropy is present throughout our study regions, with substantial lateral variability at shorter scales. As with Fig. 6, there is good agreement between the *ScS-S* and *S-SKS* data sets. Fig. 10b shows the cap-averaged anisotropy (cap radius $= 5^\circ$) after distribution along the D″ wavepaths as was done for the velocity heterogeneity estimates. There is some intermingling of split signals and apparently unsplit signals, but overall there is relatively uniform 0.5–1% anisotropy in D″ throughout the region. This map can be compared to that produced under Alaska by Garnero and Lay (1997), which indicated a comparably extensive region of about 1% VTI. As with our δV_S estimates, streaking along ray paths is present, but these maps allow us to compare our heterogeneity and anisotropy estimates.

4.3. Correlation between heterogeneity and anisotropy

Previous work has raised the issue of the relationship between velocity heterogeneity and anisotropy. For example, Maupin (1994) showed that SV_{diff} amplitudes depend on D″ anisotropy. Thus isotropic structural studies using amplitudes of core grazing

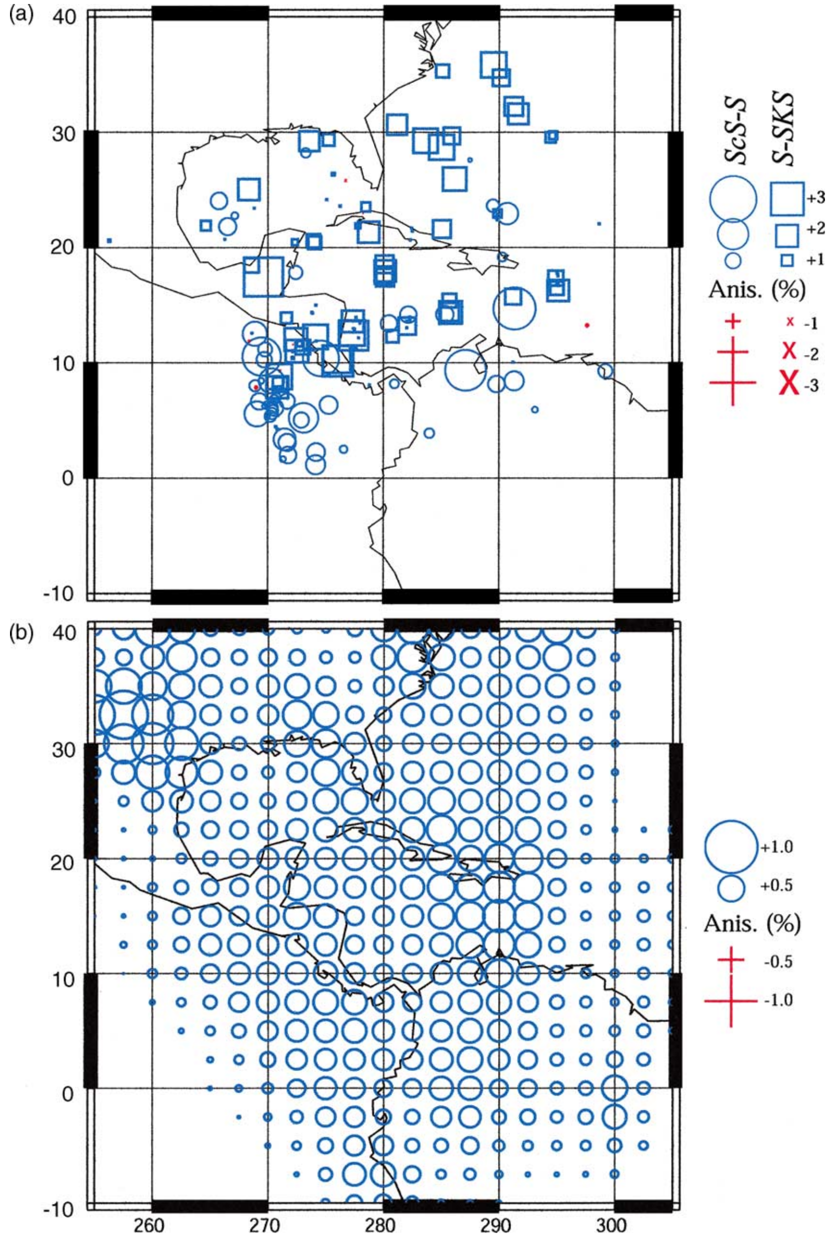

Fig. 10. (a) Shear-wave splitting measurements of Fig. 5c and d have been used to estimate D″ anisotropy strength, and are plotted at the CMB bounce (or mid-) points for *ScS* (circles and crosses) or S_{diff} (squares and Xs). Positive values (blue) correspond to data have *SH* faster that *SV*, which dominates our data set. (b) Gaussian cap-averaging of anisotropy estimates of (a) distributed along PREM-predicted D″ paths.

shear waves (e.g., Ritsema et al., 1997; Kuo, 1999) may inadvertently map anisotropy into heterogeneity. In a related effort, we compare our isotropic heterogeneity estimates to our anisotropy strength estimates. First, we compare inferred anisotropy and heterogeneity for all event-station pairs where both the differential time (*ScS-S*, or *S-SKS*) and shear wave splitting (*ScS*, or S/S_{diff}) were measured (Fig. 11a). There is a suggestion of anisotropy and heterogeneity being better correlated for S arrivals than for ScS. This might be expected since S_{diff} paths in D″ are much longer than those of ScS (e.g., Fig. 2). But in general, there is no compelling trend, except that our region contains high velocities and $V_{\mathrm{SH}} > V_{\mathrm{SV}}$ anisotropy.

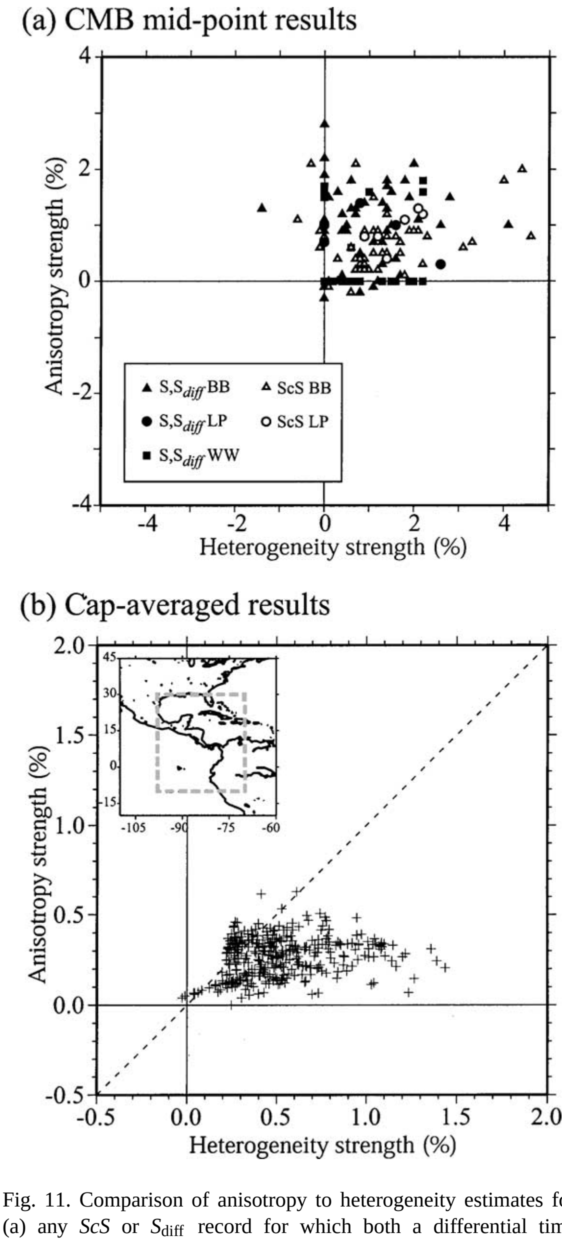

Fig. 11. Comparison of anisotropy to heterogeneity estimates for (a) any ScS or S_{diff} record for which both a differential time and splitting measurement was made, and (b) the cap averaged anisotropy and heterogeneity distributions, for every cell of a $1^\circ \times 1^\circ$ grid, for the dashed region in the inset map.

We further assess any possible correlation for the portion of our study area containing the highest density of path coverage (Fig. 11b). We correlate the anisotropy and heterogeneity estimates for each $1^\circ \times 1^\circ$ grid point of the cap-averaged values. This yields less scatter, and a weak correlation is found between the smoothed heterogeneity and anisotropy strengths for the region. This trend is weak, and does not clearly demonstrate that increased heterogeneity coincides with increased anisotropy. We are limited due to our simple methods of heterogeneity and anisotropy estimation, which depend on several assumptions. A further complication is the fact that this region shows strong 3D variability in heterogeneity. At a minimum, we can say with certainty that the entire region beneath Central America and the Caribbean, spanning an area of $1500\,\mathrm{km}^2$, has strong and variable heterogeneity and anisotropy in D″. Future work should pursue more localized investigations of the correspondence between velocity and anisotropy, particularly where the data sampling density is the highest, as this appears necessary to further assess the connection between the two.

5. Shear wave reflections off of high velocities in D″

5.1. Documenting Scd observations

Many of our ScS-S data have very good signal quality, permitting an investigation of energy reflecting above the CMB, that is, a search for the intermediate Scd arrival produced by strong radial gradients in velocity structure. We document the presence of Scd with a 3 tier classification system: Yes (Scd is clearly present), Maybe (suggestion of Scd, but the phase is either small amplitude or at a distance range where it is typically difficult to observe), and No (no evidence for Scd when it should be visible based on published discontinuity models). In this study, we do not model the individual timing or amplitude of Scd, when present. Thus we do not attempt to infer the thickness of the high-velocity layer, or the magnitude of the velocity jump at the discontinuity. Such detailed modeling requires extensive consideration of each source

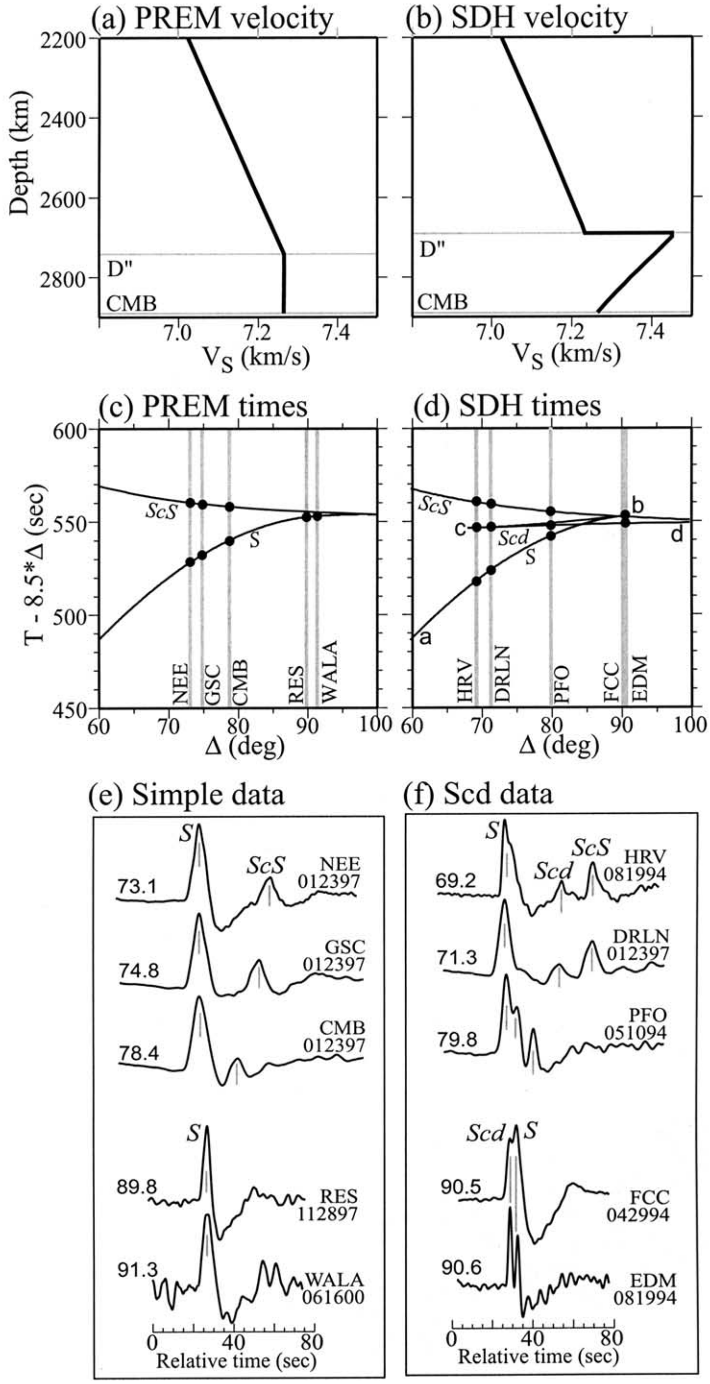

Fig. 12. (a) PREM radial shear velocity profile. (b) Shear velocity profile of model SDH of Ding and Helmberger (1997), which contains a first-order D″ discontinuity some 200 above the CMB. (c) A reduced travel-time curve for PREM, along with vertical lines that correspond to distances of example records from our data set. (d) A reduced travel time curve from model SDH, along with vertical lines that correspond to distances of example records from our data set. (e) *SH* component records compatible with the PREM model. (f) *SH* component records indicative of a discontinuity structure. An additional arrival is present in the latter seismograms.

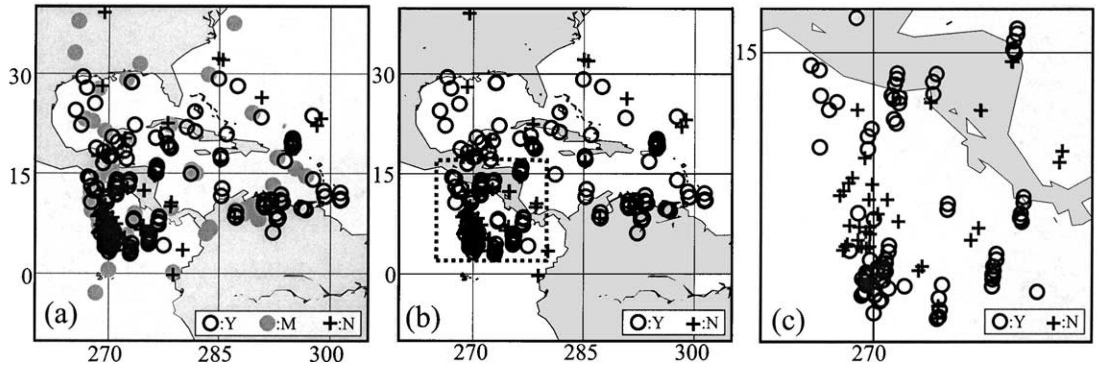

Fig. 13. (a) Observations of *Scd* are denoted by open circles at the projected D″ reflection point (Yes, 'Y'). Records lacking evidence for *Scd* are represented by the crosses (No, 'N'), and records with an intermediate arrival to *S* and *ScS*, but lower quality, are shown as solid gray circles (Maybe, 'M'). (b) Same as (a) except all Maybe's are omitted. (c) A zoom of the dotted region in (b), which illustrates small-scale coherency to the *Scd* occurrence and absence.

and receiver; however, we draw upon our past experience of modeling data and synthetic seismograms, as well as receiver structure analyses, in order to assess which waveforms show clear evidence of *Scd* arrivals or not. Discontinuity structures are characterized by an abrupt increase in velocity at the top of D″ (Fig. 12b). In models lacking a discontinuity (as in Fig. 12a), the travel time curve for *S* and *ScS* is simple (Fig. 12c), compared to the additional "*cd*" triplication branch for discontinuity structures (Fig. 12d). Data from key distances that lack or possess clear *Scd* arrivals (Fig. 12e and f, respectively) are shown as well. Systematic moveout of *Scd* with distance, as well as inspection of *S* data at all available distances help rule out misidentification of source or receiver effects as *Scd*.

Of the 297 data, we were able to utilize for investigation of *Scd* presence, 171 recordings (57%) showed very clear *Scd* detections, 69 (23%) showed probable evidence, and 57 lacked any evidence for an arrival whatsoever (19%). These Y/M/N assessments are plotted at the *ScS* CMB reflections points in Fig. 13. Evidence for an *Scd* arrival is apparent throughout the study region (Fig. 13a). If only the "Yes" and "No" identifications are retained, then positive *Scd* identifications amount to 75% of the data set (Fig. 13b). This is similar to that reported for other D″ regions exhibiting evidence for a shear wave discontinuity (e.g., 80% of the data used by Gaherty and Lay (1992) showed a clear *Scd* beneath Eurasia). Zooming into a portion of Fig. 13b (shown in Fig. 13c) illustrates that geographically coherent trends in the Yes/No data are present: a group of over 20 records lacking *Scd* evidence cluster off the west coast of Nicaragua. This raises several possibilities, which include: the D″ discontinuity has short scale lateral variations in (a) its existence, (b) its sharpness, and/or (c) its topography (i.e., D″ thickness), which result in "holes" in the reflected wavefield. Past studies have certainly noted strong lateral variations in the height of the D″ reflector (e.g., see Gaherty and Lay, 1992; Kendall and Shearer, 1994; Kendall and Nangini, 1996; Wysession et al., 1998; Garnero, 2000), often with similar presence/absence ratios that we document here.

While many possible explanations for arrivals between *ScS* and *S* exist (e.g., Young and Lay, 1987; Gaherty and Lay, 1992), systematic distance moveout of *Scd* favors a D″ reflector as the simplest, most likely explanation (e.g., in a search for scatterers Lay and Young (1996) found that a deep contiguous layer best explained the timing of arrivals between *ScS* and *S*). There are a few waveforms that may indicate greater complexity than expected for a single deep mantle reflector, but in general, if one allows for moderate variability in *Scd*-*S* timing, the consistency of the waveform evidence for triplication arrivals is very marked.

5.2. Correlating Scd occurrence with anisotropy and heterogeneity

Recognizing that a simple bimodal characterization of the D″ discontinuity presence is intrinsically

Table 2
Correlation of heterogeneity or anisotropy with *Scd* locations (see text for details)

Scd present?	Avg. δV_S (# data)	Avg. δV_S (cap avg.)	Avg. Anisot. (# data)	Avg. Anisot. (cap avg.)
Yes	1.41% (75)	0.76%	0.53% (32)	0.31%
No	1.08% (16)	0.72%	1.07% (9)	0.31%

limited, we compare Fig. 13 with Figs. 6 and 10. For our best quality data, a mild trend suggests that *Scd* observations occur in higher velocity and weaker anisotropy regions. Table 2 shows several comparisons for records that either do or do not display *Scd*. The average of the shear velocity heterogeneity estimates at all *Scd* "Yes" locations is higher than that for the *Scd* "No" locations, for both the δV_S estimates for each record and mildly for the more smoothly varying cap averaged δV_S estimates (Table 2). The average of anisotropy estimates for each record, however, are higher for the *Scd*—"No" locations. The cap-averaged anisotropy is apparently too smooth: no difference is apparent for the *Scd* Yes or No locations. Splitting observations are clearly observed in regions where no *Scd* arrival is detected in the raw data. While these regions warrant more detailed investigation this does indicate that the two phenomena may be decoupled. Certainly more work is required in this area.

6. Discussion

In this study, we observe relatively uniform structure throughout a study region of roughly 1500 km^2 dimension. Shear velocities in the D″ layer are uniformly fast throughout the region to the limit of our spatial resolution, and there is anisotropy within and a shear velocity discontinuity at the top of the D″ layer over the entire region. Evidence for D″ heterogeneity at smaller scales is certainly present, e.g., see Fig. 6b. In particular, there are regions with scales of 500–700 km of particularly fast material in D″, surrounded by a more subdued high-velocity background. We assumed a 250 km thick D″ layer in our imaging. This potentially introduces bias in some of our results for shorter distance *S* data (e.g., 85–90°) since those data may sample above the top of a 250 km thick D″. The bias takes form in two ways: (1) erroneously short predicted D″ paths can result in overestimated heterogeneity and anisotropy predictions if D″ is, in fact, thicker than we assume, and (2) data with *S* bottoming depths above the 250 km level are not incorporated here (these data may contain valuable information if a thicker layer is present, or if ray paths are significantly different than for PREM). With most of our data located at distances where the paths bottom deeper than 250 km above the CMB, the overall effects of these concerns should be minor. We note that anisotropy has been proposed to exist at shallower depths relative to the CMB in other regions, such as in the Indian Ocean (region 4, Fig. 1): Ritsema (2000) suggests a sudden onset of anisotropy around 350 km above the CMB. Fig. 5c shows that some data possibly bottoming above our 250 km layer do display shear wave splitting. However, if there is a strong radial velocity gradient at the top of D″, many S ray paths will actually cluster near the top of D″, well below the turning points predicted for the PREM model. Localized, detailed modeling is the only reliable way to overcome these competing effects.

Our maps of shear velocity heterogeneity, anisotropy, and discontinuity indicate that the causes of these properties must involve lateral dimensions of roughly 1500 km^2 (Fig. 14). This is an important constraint, and supports the findings of both large scale tomographic models and work on other localized regions of D″. Large-scale boundary layer features such as a compositionally distinct layer, a phase change, or a repository of subducted materials beneath active downwellings are all compatible with large-scale provinces being present at the base of the mantle. The dynamical notion that a compositionally distinct layer should actually be thinned under regions of downwelling, and the lack of a candidate phase change in major lower mantle minerals tend to reduce the viability of those models. Lower mantle penetration of lithospheric slabs remains contentious, but does have the appealing attribute of accounting for the mid-mantle high-velocity regions found beneath zones of extensive slab subduction over the past 150 m.y. The intrinsic large dimensions of subducted

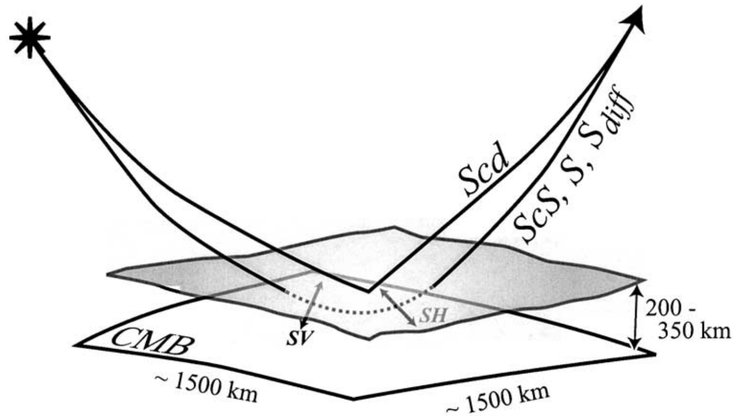

Fig. 14. A schematic showing the important dimensions and ray geometries of this study. A D″ reflector, anisotropy, and high-wave speeds are all apparent over a minimum dimension of roughly 1500 km^2. Strong variations in D″ thickness, velocity, and anisotropy certainly overprint this large scale structure.

slabs may account for the large-scale structure found in our D″ study area if slab material has penetrated to D″ and ponded at the base of the mantle. We do believe that the seismic evidence for connectivity of slabs from the surface all the way to D″ is scant, but the one region for which nearly all tomographically derived shear velocity structures show the best evidence for high-velocity tabular structures extending down to D″ is beneath the Caribbean (see Grand et al., 1997). Assuming that there is sufficient thermal anomaly present to account for the volumetric shear velocity anomaly, one must then consider whether this provides an explanation for the anisotropy and discontinuity features.

Many discussions of the origin of D″ anisotropy are based on the hypothesis of subducted material reaching D″ (e.g., Kendall and Silver, 1996; McNamara et al., 2002). Fig. 15 summarizes some conceptual models proposed in the literature. Recently, a geodynamical study has attributed lower mantle strain associated with subduction to the cause of seismic anisotropy (McNamara et al., 2001, 2002). Fig. 15a and b is a simplification of this possibility: high strains some 200–350 km above the CMB result in anisotropy and produce the *Scd* reflection as well. Slab contortions may also be possible (Fig. 15c and d), but to explain our data there must be significant contiguous nature to the anisotropy (as in Fig. 14). High strains in D″ may also be produced below slabs that do not reach the CMB (Fig. 15e), which does not preclude the existence of a chemically distinct reservoir as suggested by Kellogg et al. (1999) (Fig. 15f). An alternative mechanism for generating anisotropy is some form of low-velocity lamellae in D″. Kendall and Silver (1996, 1998) argued for delamination of former oceanic crust from the slab (Fig. 15g), which may partially melt and fold over to produce a net SPO. This seems unlikely to account for an extensive region of anisotropy as we observe. Other possibilities include a phase change causing the D″ discontinuity (Sidorin et al., 1999), and also deep mantle scatterers aligned by shear flow giving seismic anisotropy (e.g., Cormier, 2000).

The observation that similar spatially extensive regions of shear wave velocity heterogeneity, anisotropy, and discontinuity structure are found in D″ regions that lack clear continuity of slab-like structures extending throughout the lower mantle (such as is the case under Alaska) does undermine the notion of a slab related origin for these phenomena. The lack of clear correlation between the presence of anisotropy and the discontinuity also raises questions about any causal linkage of the two. Yet one cannot help but be intrigued by the general correlation between zones of down-welling and anomalous D″ structures.

Our current results do not uniquely establish the cause of the heterogeneity in D″ beneath Central America; however, the laterally extensive nature of the D″ attributes that we detect supports the notion that the boundary layer structure constitutes a major feature of the deep mantle, not a localized anomaly.

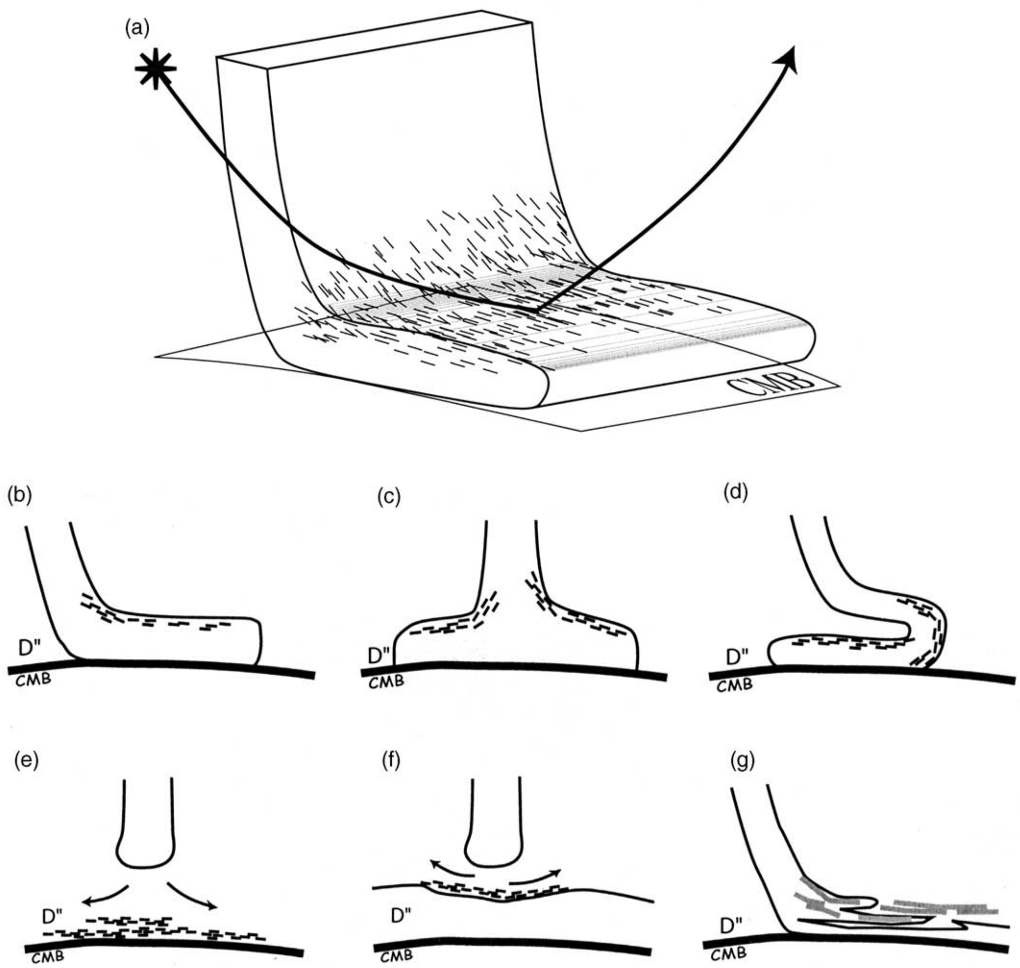

Fig. 15. Scenarios that relate downwelling lithospheric slabs to deep mantle shear velocity heterogeneity, anisotropy and discontinuity structure. See text for details.

When combined with large-scale features such as the low velocity regions underlying the Central Pacific and southern Africa, it is clear that the boundary layer at the base of the mantle is indeed as complex as the surface boundary layer is known to be. Finer scale analyses continue to be required to elucidate the physics and chemistry responsible for our observations. Within the broad region studied in the current paper, we can identify several specific target areas for such detailed analyses: (1) the region of spatially coherent "No *Scd*" observations west of Central America in Fig. 13d; (2) the zone of particularly fast structure below Nicaragua in Fig. 6b; and (3) the region of mixed anisotropy observations below the Caribbean in Fig. 10a, which include observations inconsistent with VTI. Detailed investigations of all of these subregions will soon be completed.

7. Conclusions

The lowermost mantle beneath the Caribbean and Central America exhibits wide-spread high-shear wave velocities, pervasive shear wave anisotropy that is largely compatible with VTI orientation, and a laterally extensive D″ discontinuity structure.

Differential travel times *ScS-S* and *S-SKS* reveal that the highest D″ velocities (up to 5% fast relative to PREM) are localized to a region beneath Central America, approximately 500–700 km in lateral dimension. Evidence for smaller scale heterogeneity is also present, with reduced velocities on the order of 1% fast underlying the Caribbean and 3–4% high velocities under northern South America. The D″ region beneath the western Atlantic off the U.S. coast has only moderately fast velocities as well. Shear wave splitting in *S* (or S_{diff}) and *ScS* has been used to map anisotropy strength throughout the study area. A weak correlation between heterogeneity and anisotropy is present. Evidence for *Scd*, a seismic wave that reflects off of the high-velocity D″ layer, is found throughout our study region. Some localized zones (100–200 km in extent) lack clear evidence for *Scd* in the waveforms, possibly due to small-scale topographical and/or volumetric variability in the otherwise pervasive discontinuity at the top of D″ in this region. These phenomena persist over extensive lateral dimensions ($\sim$1500 km^2), which provide an important constraint for interpretations of the cause of these observations.

Acknowledgements

We thank Michael Bostock and Harley Benz, who graciously supplied CNSN and USNSN data, respectively. Lizz Leon helped collect IRIS FARM data. Constructive reviews by Karen Ficsher and Steve Grand helped to improve the paper Many figures were drafted using GMT, written by Paul Wessel and Walter Smith. This research was supported by NSF grants EAR-9814554, EAR-9996302 (EG) and EAR-0125595 (TL).

References

Albarede, F., Van Der Hilst, R.D., 1999. New mantle convection model may reconcile conflicting evidence. EOS 80, 535–539.

Bokelmann, G.H.R., Silver, P.G., 1993. The Caribbean anomaly: short-wavelength lateral heterogeneity in the lower mantle. Geophys. Res. Lett. 10, 1131–1134.

Castle, J.C., Creager, K.C., Winchester, J.P., 2000. Shear wave speeds at the base of the mantle. J. Geophys. Res. 105, 21543–21557.

Cormier, V.F., 2000. D″ as a transition in the heterogeneity spectrum of the lowermost mantle. J. Geophys. Res. 105, 16193–16205.

Ding, X., Helmberger, D.V., 1997. Modeling D″ structure beneath Central America with broadband seismic data. Phys. Earth Planet. Int. 101, 245–270.

Dziewonski, A.M., Anderson, D.L., 1981. Preliminary reference earth model. Phys. Earth Planet Int. 25, 297–356.

Fisher, J.L., Wysession, M.E., Fischer, K.M., 2003. Small-scale lateral variations in D″ attenuation and velocity structure. Geophys. Res. Lett. 30, 1435–1439.

Fouch, M.J., Fischer, K.M., Wysession, M.E., 2001. Lowermost mantle anisotropy beneath the Pacific: imaging the source of the Hawaiian plume. Earth Planet. Sci. Lett. 190, 167–180.

Gaherty, J.B., Lay, T., 1992. Investigation of laterally heterogeneous shear velocity structure in D″ beneath Eurasia. J. Geophys. Res. 97, 417–435.

Garnero, E.J., 2000. Lower mantle heterogeneity. Ann. Rev. Earth Planetary Sci. 28, 509–537.

Garnero, E.J., Helmberger, D.V., Grand, S.P., 1993. Preliminary evidence for a lower mantle shear wave velocity discontinuity beneath the central Pacific. Phys. Earth Planet. Int. 79, 335–347.

Garnero, E.J., Lay, T., 1997. Lateral variations in lowermost mantle shear wave anisotropy beneath the north Pacific and Alaska. J. Geophys. Res. 102, 8121–8135.

Garnero, E.J., Lay, T., 1998. Effects of D″ anisotropy on seismic velocity models of the outermost core. Geophys. Res. Lett. 25 (13), 2341–2344.

Grand, S.P., Van Der Hilst, R.D., Widiyantoro, S., 1997. Global seismic tomography: a snapshot of convection in the Earth. GSA Today 7, 1–7.

Grand, S.P., 2002. Mantle shear-wave tomography and the fate of subducted slabs. Phil Trans R. Soc. Lond. A, 360, 2475–2491.

Gu, Y.J., Dziewonski, A.M., Su, W., Ekström, G., 2001. Models of the mantle shear velocity and discontinuities in the pattern of lateral heterogeneities. J. Geophys. Res. 106, 11169–11199.

Jordan, T.H., Lynn, W.S., 1974. A velocity anomaly in the lower mantle. J. Geophys. Res. 79, 2679–2685.

Karato, S.I., 1993. Importance of anelasticity in the interpretation of seismic tomography. Geophys. Res. Lett. 20, 1623–1626.

Karato, S.I., 1998. Some remarks on the origin of seismic anisotropy in the D″ layer. Earth Planets Space 50, 1019–1028.

Karason, H., Van der Hilst, R.D., 2001. Tomographic imaging of the lowermost mantle with differential times of refracted and diffracted core phases (PKP, P-diff). J. Geophys. Res. 106, 6569–6587.

Karki, B.B., Wentzcovitch, R.M., De Gironcoli, S., Baroni, S., 1999. First-principles determination of elastic anisotropy and wave velocities of MgO at lower mantle conditions. Science 286, 1705–1709.

Kellogg, L.H., Hager, B.H., Van der Hilst, R.D., 1999. Compositional stratification in the deep mantle. Science 283, 1881–1884.

Kendall, J.M., 2000. Seismic anisotropy in the boundary layers of the mantle. In: Karato, S., Forte, A.M., Liebermann, R.C., Masters, G., Stixrude, L. (Eds.), Earth's Deep Interior: Mineral Physics and Tomography From the Atomic to the Global Scale. American Geophysical Union, Washington, DC, USA, pp. 133–159.

Kendall, J.M., Shearer, P.M., 1994. Lateral variations in D″ thickness from long-period shear wave data. Geophys. Res. Lett. 99, 11575–11590.

Kendall, J.M., Nangini, C., 1996. Lateral variations in D″ below the Caribbean. Geophys. Res. Lett. 23, 399–402.

Kendall, J.M., Silver, P.G., 1996. Constraints from seismic anisotropy on the nature of the lowermost mantle. Nature 381 (6581), 409–412.

Kendall, J.M., Sliver P.G., 1998. Invertigating causes of D″ anisotropy. In: Gurnis, M., Wysession, M., Knittle, E., Buffet, B. (Eds.), The Core–Mantle Boundary Region. American Geophysical Union, Washington, DC, USA, pp. 97–118.

Kuo, B.Y., 1999. Amplitude of S_{diff} across Asia: effects of velocity gradient and Q_S in the D″ regions and the asphericity of the mantle. Earth Planet. Sci. Lett. 173, 101–112.

Kuo, B.Y., Garnero, E.J., Lay, T., 2000. Tomographic Inversion of S-SKS times for shear wave velocity heterogeneity in D″: degree 12 and hybrid models. J. Geophys Res. 105, 28139–28157.

Lay, T., 1983. Localized velocity anomalies in the lower mantle. Geophys. J.R. Astron. Soc. 72, 483–516.

Lay, T., Helmberger, D.V., 1983a. A lower mantle *S*-wave triplication and the shear velocity structure of D″. Geophys. J.R. Astron. Soc. 75, 799–838.

Lay, T., Helmberger, D.V., 1983b. The shear wave velocity gradient at the base of the mantle. J. Geophys. Res. 88, 8160–8170.

Lay, T., Young, C.J., 1996. Imaging scattering structures in the lower mantle by migration of long-period *S* waves. J. Geophys. Res. 101, 20,023–20,040.

Lay, T., Young, C.J., 1991. Analysis of SV waves in the cores penumbra. Geophys. Res. Lett. 18, 1373–1377.

Lay, T., Garnero, E.J., Young, C.J., Gaherty, J.B., 1997. Scale-lengths of heterogeneity at the base of the mantle from S-wave differential times. J. Geophys. Res. 102, 9887–9909.

Lay T., Garnero E.J., Williams Q., Kellogg L., Wysession M.E., 1998a. Seismic wave anisotropy in the D″ region and its implications. In: Gurnis, M., Wysession, M., Knittle, E., Buffet, B. (Eds.), Core–Mantle Boundary Region. American Geophysical Union, Washington, DC, USA, pp. 229–318.

Lay, T., Williams, Q., Garnero, E.J., 1998b. The core–mantle boundary layer and deep Earth dynamics. Nature 392 (6675), 461–468.

Lithgow-Bertelloni, C., Richards, M.A., 1998. The dynamics of cenozoic and mesozoic plate motions. Rev. Geophys. 36, 27–78.

Mainprice, D., Barruol G., Ben Ismail W., 2000. The seismic anisotropy of the Earth's mantle: from single crystal to polycrystal. In: Karato, S., Forte, A.M., Liebermann, R.C., Masters, G., Stixrude, L. (Eds.), Earth's Deep Interior: Mineral Physics and Tomography From the Atomic to the Global Scale., American Geophysical Union, Washington, DC, USA.

Masters G., Bolton H., Dziewonski A.M., Laske G., 2000. The relative behavior of shear velocity, bulk sound speed, and compressional velocity in the mantle: implications for chemical and thermal structure. in: Karato, S., Forte, A.M., Liebermann, R.C., Masters, G., Stixrude, L. (Eds.), Earth's Deep Interior: Mineral Physics and Tomography From the Atomic to the Global Scale. American Geophysical Union, Washington, DC, USA, pp. 63–87.

Matzel, E., Sen, M.K., Grand, S.P., 1996. Evidence for anisotropy in the deep mantle beneath Alaska. Geophys. Res. Lett. 23, 2417–2420.

Maupin, V., 1994. On the possibility of anisotropy in the D″ layer as inferred from the polarization of diffracted S waves. Phys. Earth Planet. Int. 87, 1–32.

McNamara, A.K., Karato, S.I., Van Keken, P.E., 2001. Localization of dislocation creep in the lower mantle: implications for the origin of seismic anisotropy. Earth Planet. Sci. Lett. 191, 85–99.

McNamara, A.K., Van Keken, P.E., Karato, S.I., 2002. Development of anisotropic structure in the Earth's lower mantle by solid-state convection. Nature 416, 310–314.

Megnin, C., Romanowicz, B., 2000. The three-dimensional shear velocity structure of the mantle from the inversion of body, surface, and higher-mode waveforms. Geophysical Journal International 143, 709–728.

Mitchell, B.J., Helmberger, D.V., 1973. Shear velocities at base of mantle from observations of *S* and *ScS*. J. Geophys. Res. 78, 6009–6020.

Moore M.M., Garnero E.J., Lay T., Williams Q., 2003. Synthesizing shear wave splitting and waveform complexity for lowermost mantle structures with low-velocity lamellae and transverse isotropy, J. Geophys. Res., in press.

Montagner, J.-P., 1998. Where can seismic anisotropy be detected in the Earth's mantle? In boundary layers.... Pure Appl. Geophys. 151, 223–256.

Pulliam, J., Sen, M.K., 1998. Seismic anisotropy in the core–mantle transition zone. Geophys. J. Int. 135, 113–128.

Reasoner, C., Revenaugh, J., 1999. Short-period P wave constraints on D″ reflectivity. J. Geophys. Res. 104, 955–961.

Ritsema, J., 2000. Evidence for shear velocity anisotropy in the lowermost mantle beneath the Indian Ocean. Geophys. Res. Lett. 27 (7), 1041–1044.

Ritsema, J., Van Heijst, H.J., 2000. Seismic imaging of structural heterogeneity in Earth's mantle: evidence for large-scale mantle flow. Science Progress 83, 1,925.

Ritsema, J.E., Garnero, E.J., Lay, T., 1997. A strongly negative shear velocity gradient and lateral variability in the lowermost mantle beneath the Pacific. J. Geophys. Res. 102, 20,395–20,411.

Ritsema, J., Lay, T., Garnero, E.J., Benz, H., 1998. Seismic anisotropy in the lowermost mantle beneath the Pacific. Geophys. Res. Lett. 25, 1229–1232.

Romanowicz, G., Gung, Y.C., 2002. Superplumes from the core–mantle boundary to the lithosphere: Implications for hear flux. Science 296, 513–516.

Russell, S., Lay, T., Garnero, E.J., 1998. Seismic evidence for small-scale dynamics in the lowermost mantle at the root of the Hawaiian hotspot. Nature 369, 255–257.

Russell, S.A., Lay, T., Garnero, E.J., 1999. Small-scale lateral shear velocity and anisotropy heterogeneity near the core–mantle boundary beneath the central Pacific imaged using broadband *ScS* waves. J. Geophys. Res 104, 13183–13199.

Russell, S.A., Reasoner, C., Lay, T., Revenaugh, J., 2001. Coexisting shear- and compressional-wave seismic velocity discontinuities beneath the central Pacific. Geophys. Res. Lett. 28, 2281–2284.

Savage, M.K., 1999. Seismic anisotropy and mantle deformation: what have we learned from shear wave splitting. Rev. Geophys. 37, 65–106.

Sidorin, I., Gurnis, M., Helmberger, D.V., 1999. Dynamics of a phase change at the base of the mantle consistent with seismological observations. J. Geophys. Res. 104, 15,005–15,023.

Silver, P.G., 1996. Seismic anisotropy beneath the continents: probing the depths of geology. Ann. Rev. Earth Panel. Sci. 24, 385–432.

Silver, P.G., Chan, W.W., 1988. Implications for continental structure and evolution from seismic anisotropy. Nature 335, 34–39.

Tackley, P., 2000. Mantle convection and plate tectonics: Toward an integrated physical and chemical theory. Science 288, 2002–2007.

Thomas, C., Kendall, J.M., 2002. The lowermost mantle beneath northern Asia. Part II. Evidence for lower-mantle anisotropy. Geophys. J. Int. 151, 296–308.

Tkalcic, H., Romanowicz, B., 2001. Short scale heterogeneity in the lowermost mantle: insights from PcP-P and ScS-S data. Earth Planet. Sci. Lett. 201, 57–68.

Van der Hilst, R.W., Widiyantoro, S., Engdahl, E.R., 1997. Evidence for deep mantle circulation from global tomography. Nature 386, 578–584.

Valenzuela Raúl W., Michael E. Wysession, 1998. Illuminating the base of the mantle with diffracted waves. In: Gurnis, M., Wysession, M.E., Knittle, E., Buffett, B.A. (Eds), The Core–Mantle Boundary Region, Geodynamics Series no. 28, American Geophysical Union, Washington, DC,, pp. 57–71.

Vinnik, L., Farra, F., Romanowicz, B., 1989. Observational evidence for diffracted *SV* in the shadow of the Earth's core. Geophys. Res. Lett. 16, 519–522.

Vinnik, L., Romanowicz, B., Lestunff, Y., Makeyeva, L., 1995. Seismic anisotropy in the D″ layer. Geophys. Res. Lett. 22 (13), 1657–1660.

Vinnik, L., Breger, L., Romanowicz, B., 1998. Anisotropic structures at the base of the Earth's mantle. Nature 393 (6685), 564–567.

Weber, M., Davis, J.P., 1990. Evidence of a laterally variable lower mantle structure from *P*- and *S*-waves. Geophys. J. Int. 102, 231–255.

Wysession, M.E., 1996. Imaging cold rock at the base of the mantle: The sometimes fate of Slabs? In: Bebout, G.E., Scholl, D., Kirby, S., Platt, J.P. (Eds.), Subduction: Top to Bottom. AGU, Washington, DC, pp. 369–384.

Wysession, M., Lay T., Revenaugh J., Williams Q., Garnero E.J., Jeanloz R., Kellogg L., 1998. The D″ discontinuity and its implications. In: The Core–mantle Boundary, AGU, Washington, DC, pp. 273–298.

Wysession, M.E., Fischer, K.M., Al-eqabi, G.I., Shore, P.J., Gurari, I., 2001. Using MOMA broadband array *ScS*-*S* data to image smaller-scale structures at the base of the mantle. Geophys. Res. Lett. 28, 867–870.

Yamazaki, D., Karato, S.-I., 2002. Fabric development in (Mg,O) during large strain shear deformation: implications for seismic anisotropy in Earth's lower mantle. Phys. Earth. Planet. Int. 131, 251–267.

Young, C.J., Lay, T., 1987. Evidence for a shear velocity discontinuity in the lower mantle beneath India and the Indian Ocean. Phys. Earth Planet. Int. 49, 37–53.

Young, C.J., Lay, T., 1990. Multiple phase analysis of the shear velocity structure in the D″ region beneath Alaska. J. Geophys. Res. 95, 17,385–17,402.

Zhang, J., Lay, T., 1984. Investigation of a lower mantle shear wave triplication using a broadband array. Geophys. Res. Lett. 11, 620–623.